Geophysical Journal International

The Al Hoceima earthquake sequence of 1994, 2004 and 2016: Stress transfer and poro-elasticity in the Rif and Alboran Sea region

Journal:	*Geophysical Journal International*
Manuscript ID	GJI-S-16-0794.R2
Manuscript Type:	Research Paper
Date Submitted by the Author:	n/a

Complete List of Authors:	Kariche, Jugurtha; Institut de physique du globe de Strasbourg, Deformation Active; Universite des Sciences et de la Technologie Houari Boumediene, Géophysique Meghraoui, Mustapha; Institut de physique du globe de Strasbourg, Deformation Active Timoulali, Youssef; University Mohamed V, Rabat-Agdal, Morocco, Dept. of Geophysics Cetin, Esra; Mugla Sitki Kocman Universitesi, Dept. of Geological Engineering Toussaint, Renaud; IPGS, CNRS, Université de Strasbourg,

Keywords:	Dynamics: seismotectonics < TECTONOPHYSICS, Neotectonics < TECTONOPHYSICS, Fractures, faults, and high strain deformation zones < TECTONOPHYSICS, Seismicity and tectonics < SEISMOLOGY

The Al Hoceima earthquake sequence of 1994, 2004 and 2016: Stress transfer and poro-elasticity in the Rif and Alboran Sea region

J. Kariche [1, 2], M. Meghraoui [1], Y. Timoulali [3], E. Cetin [1, 4], and R. Toussaint [1]

[1]Institut de Physique du Globe de Strasbourg, Université de Strasbourg/EOST, CNRS-UMR7516, Strasbourg, France.
[2] USTHB, Laboratoire de Geophysique, FSTGAT, B.P. 32 El Alia, 16111 Bab Ezzouar, Algiers, Algeria..
[3] Dept. of Geophysics, University Mohamed V, Rabat-Agdal, Morocco.
[4] Dept. of Geological Engineering, Mugla Sitki Kocman University

July 2017

Abstract

The 25 January 2016 earthquake (Mw 6.3) follows in sequence from the 26 May 1994 earthquake (Mw 6.0) and the 24 February 2004 earthquake (Mw 6.4) in the Rif Mountains and Alboran Sea. The earlier two seismic events which were destructive took place on inland conjugate faults, and the third event occurred on an offshore fault. These earthquake sequences occurred within a period of 22 years at ~25 km distance and 11 – 16-km-depth. The three events have similar strike-slip focal mechanism solutions with NNE-SSW trending left lateral faulting for the 1994 and 2016 events and NW-SE trending right-lateral faulting for the 2004 event. This shallow seismic sequence offers the possibility a) to model the change in Coulomb Failure Function (ΔCFF with low μ' including the pore pressure change) and understand fault-rupture interaction, and b) to analyse the effect of pore-fluid on the rupture mechanism, and infer the clock-time advance. The variation of static stress change has a direct impact on the mainshock, aftershocks and related positive lobes of the 2004 earthquake rupture with a stress change increase of 0.7 – 1.1 bar. Similarly, the 2004 mainshock and aftershocks indicate loading zones with a stress change (> 0.25 bar) that includes the 2016 earthquake rupture. The tectonic loading of 19 - 24 nanostrain/yr obtained from the seismicity catalogue of Morocco is comparable to the 5.0×10^{17} N.m/yr seismic strain release in the Rif Mountains. The seismic sequence is apparently controlled by the poro-elastic properties of the seismogenic layer that depend on the undrained and drained fluid condition. The short interseismic period between mainshocks and higher rate of aftershocks with relatively large magnitudes (4< Mw <5.5) implies the pore-fluid physical effect in an undrained and drained conditions. The stress-rate ranges between 461 - 582 Pa/yr with a ΔCFF of 0.2 – 1.1 bar. The computed clock-time advance reaches 239 ±22 years in agreement with the ~10 years delay between mainshocks. The calculated static stress change of 0.9 – 1.3 bar, under pore-fluid

stimulus added with well-constrained geodetic and seismic strain rates are critical for any seismic hazard assessment.

Introduction

Three significant earthquakes have occurred on 26/05/1994 (Mw 6.0), 24/02/2004 (Mw 6.4) and 25/01/2016 (Mw 6.5) in the Rif Mountains of Morocco – southern Alboran Sea area within a period of 22 years (Figure 1). The earlier two earthquakes caused severe damage due to their location inland, but the third offshore event was only felt on the nearby Moroccan coastline. Aftershock distribution (El Alami et al., 1998; Bezzeghoud and Buforn, 1999) and surface deformation as deduced from InSAR (Akoglu et al., 2006; Cakir et al., 2006; Tahayt et al., 2009), indicate that the 1994 and 2004 events occurred on NNE-SSW and NW-SE trending conjugate strike-slip faults, respectively. The 2016 event located about 20 km offshore is associated with a NNE-SSW trending rupture with a similar mechanism to the 1994 event. This seismic sequence is unusual in the North Africa active zones because earthquake ruptures are within ~25 km area and the time interval between mainshocks is about 10 – 12 years.

In this paper, we first present the seismic sequence and suggest a fault rupture interaction using Coulomb modelling on fixed planes. Secondly, the computation using optimally oriented planes is added to constrain aftershocks distribution. The three mainshocks and related aftershocks appear to be closely related and their location implies a stress transfer with triggering. We show that the modelled stress distribution and seismicity rate change suggest a pore-fluid effect correlated with elastic dislocation in undrained and drained conditions. The Coulomb Failure Function change (ΔCFF) and pore-fluid flow seem to control the 10-12 years recurrence of main seismic events with a clock advance. The plate boundary tectonic condition, the seismicity rate change and poro-elastic properties of the seismogenic crust seem to play a significant role in the triggering of earthquakes in the Rif Mountains and Alboran Sea.

Seismotectonic setting

The seismicity of the Rif Mountains and Alboran Sea is due to the convergence between Africa and Eurasia (Iberia) in the western Mediterranean. The E-W trending Rif Mountains run along the northern coast of Morocco forming the southern branch of the Betic-Rif arc that includes the Alboran Sea and belongs to the transpression plate boundary system in the Western Mediterranean region (Morel & Meghraoui, 1996; Meghraoui and Pondrelli, 2012). Tahayt et al. (2009) interpret the region as a trans-rotational regime applied to the Oriental Rif block with a clockwise rotation. This complex tectonic domain also results from a Neogene subdued subduction zone with lithospheric delamination where the Alboran Sea appears as an oceanic microplate (Calvert et al., 1997).

As indicated by the three mainshocks (Figure 1 and Table 1), the present-day tectonic framework of the Al Hoceima region is dominated by a strike slip fault regime where moment magnitudes do not exceed 6.5. Limited fault rupture dimensions are likely due to the local structural geology made of overthrusting nappes on highly deformed continental crustal rocks (Chalouan et al., 2008; Timoulali et al., 2013). Because of the limited number of local seismic stations in the Rif, the location of aftershocks of the 1994 and offshore 2016 earthquakes are poorly resolved, which is not the case for the 2004 earthquake (Tahayt et al., 2009).

Several authors have studied the seismicity and suggested moment tensor solutions of major earthquakes showing a NNW-SSE contraction stress regime in a predominantly strike-slip faulting domain associated with normal and thrust mechanisms (Hartzfeld et al. 1977, Cherkaoui 1992, Medina 1995, Stich et al., 2006; Stich et al 2010; Palano et al., 2013). Although the seismicity may appear diffuse in the Rif-Alboran Sea, the 1994, 2004 and 2016 seismic events reveals a clear migration of earthquake ruptures (Figure 1). The seismicity and tectonics of the region indicate a clear correlation between continental and offshore faults from both the Betics and Rif Mountains towards the Alboran Sea (Grevemeyer et al., 2015). From detailed bathymetry and seismicity distribution, Gevemeyer et al. (2015) identify a fault zone crossing the Alboran ridge at the location of the 25 January 2016 earthquake (Mw 6.5). Using InSAR Cakir et al. (2006) and Akoglu et al. (2006) constrain the coseismic earthquake surface deformation and provide the rupture parameters of the N23° E trending 1994 and N45° W trending 2004 earthquakes using elastic dislocations. They suggest that the two mainshocks occurred on blind and conjugate strike-slip faults, with left-lateral and right-lateral slip, respectively. The time series analysis of SAR data (Envisat) for seven years following the 2004 earthquake shows that postseismic deformation reaches up to 4 cm at the surface and infers 0.3 m displacement at shallow depth (< 7 km), mainly above the high coseismic slip patches which can be explained by 5.0×10^{17} N.m. (*Mw* 5.73) cumulative moment release (Cetin, 2015). The 2016 earthquake rupture, located about 20 km further north, is modelled for the source time function to obtain a strike-slip faulting mechanism with a NNE-SSW main rupture in agreement with aftershock distribution (Vallée, 2016). The three focal mechanism solutions and the 1994 and 2004 rupture geometries inferred from surface deformation are used as an input for the ΔCFF modelling (Table 1).

Modeling Al Hoceima sequence by Coulomb Failure Function

The Rif region of northern Morocco experienced a seismic sequence with three moderate to large earthquakes within 22 years. The sequence suggests earthquake triggering, fault interaction and stress transfer as observed in other earthquake areas (Hudnut et al, 1989; Stein et al., 1997). The case-study uses the applied stress change calculated as Coulomb Failure Function (ΔCFF; Reasenberg and Simpson, 1992, King et al 1994) expressed by:

$$\Delta CFF = \Delta\tau - \mu\,(\,\Delta\sigma_n - \Delta P) \qquad (1)$$

$$\Delta CFF = \Delta\tau - \mu'\,\Delta\sigma_n \qquad (2)$$

where τ is the shear stress, σ_n is the normal stress (compression positive), P is the pore fluid pressure, μ and μ' are the coefficient of friction and effective coefficient of friction, respectively, and Δ refers to changes during the earthquake.

The apparent friction is given by (Reasenberg and Simpson, 1992)

$$\mu' = \mu\,(1 - B) \qquad (3)$$

Where B is the Skempton coefficient which defines the relation between the stress change and pore pressure change (Beeler et al, 2000)

$$B = \frac{\Delta P}{\Delta\sigma_m} = 3\,\frac{\Delta P}{\Delta\sigma_{kk}} \qquad (4)$$

Where $\Delta\sigma_m$ is the mean stress change and $\Delta\sigma_{kk}$ is the sum over the diagonal elements of the stress tensor. It is important to note that for an isotropic model, the apparent friction coefficient used in triggered seismicity is defined by the combination of pore pressure and friction coefficient:

$$\mu' = \mu\,(\,1 - \frac{\Delta P}{\Delta\sigma_n}) \qquad (5)$$

Substituting (5) and (4) in (2), we obtain

$$\Delta CFF = \Delta\tau + \mu\,(\Delta\sigma_n - B\Delta\sigma_m) \qquad (6)$$

Beeler and al (2000) suggest that due to the pore fluid effect and for an isotropic poro-elastic model, the two expressions defined in (2) and (6) yield different results in some modelling configurations. The variable effective friction coefficient related to the variation of the Skempton coefficient B and the pore pressure change along the fault zone gives more realistic solutions especially at high pore pressure change than the imposed constant effective friction commonly used in the Coulomb stress modelling (see Appendixes A and B for more details). The variation of B must be considered when different porosity and different diffusive processes are present in the fault zone (Scholz, 1990). From the structural point of view, fluid migration in the host rock may occur on nearby subsidiary fractures linked to bounding faults directly related to earthquake and aftershock behavior (Kirkpatrick et al., 2008).

The cumulative moment for Al Hoceima region (inland and offshore) reaches 1.1×10^{19} N.m. since 1994, and the seismic strain release tested on a fault network reveals a low effective coefficient of friction on the fault (≤ 0.2) to model the slip rates (Negredo et al., 2002). In order to model the active tectonics of the Ibero-Maghrebian region, a strain rate of 15 - 40 nanostrain/year is obtained using slip rates on faults and GPS data (Negredo et al, 2002; Koulali et al., 2011; Palano et al., 2013). In their calculation of frictional strength, Negredo et al. (2002) assume no cohesion in the media.

In our work, the modelling is performed using Coulomb 3.4 software (Toda et al., 2011) based on the conversion of DC3D subroutines (Okada, 1992) to calculate the ΔCFF. The static stress change is computed on both fixed receiver earthquake ruptures and optimally oriented faults using an effective coefficient of friction $\mu' = 0.4$, and fault parameters summarized in Table 2. The computed stress changes are presented in Table 3 where the value of static stress change according to the receiver fault represents the ΔCFF_{max} and also expresses the Coulomb stress drop on the source faults.

In the ΔCFF modelling computed with fixed strike-slip receiver fault plane, the correlation between loading lobes and aftershock distribution suggests a close interaction between the 1994, 2004 and 2016 earthquake ruptures (Figures 2 a, b and c, Table3, Figure 3 a , Figure S1 a and b, Figure S2 and Table S1). Unlike the 2016 earthquake epicentre which is clearly within a positive CFF lobes, the 2004 earthquake location given by the InSAR analysis (Akoglu et al., 2006) is at the transition from negative to positive ΔCFF lobes. Taking the

1994 as a source fault and the 2004 rupture as a receiver fault, and using a low friction coefficient (μ' < 0.4 and for isotropic models, Figures 3a and 3b), our CFF modelling show the 2004 fault rupture clearly located in a loading zone with positive stress change.

The cumulative ΔCFF from 1994 to 2016 (Figure 2 d) explains the present-day and most important part of the seismicity and aftershock distribution and Coulomb stress drop in the Al Hoceima region. In order to analyse the relationship between the mainshocks and aftershocks distribution in detail, we model a static stress change caused by the 2004 and the 2016 earthquakes on some major aftershocks (see Table S). The modelling on fixed receiver planes suggest a stress load range between 0.5-0.8 bar for 2004 aftershock sequences with an optimal strike and dip value ranging between 207°and 298° and 66°and 84°, respectively. For the 2016 earthquake, major aftershocks are reached by a positive ΔCFF ranging between 0.1 and 0.4 bar, with an optimal value of [250° - 260°] for Strike and [40°- 45°] for Dip.

In order to take into account all aftershock sequences, we compute a static stress change on optimally oriented fault planes as this approach does not need to include the focal mechanism of each rupture. As obtained by previous works on the northern Morocco tectonics (Medina et al., 1995, Akoglu et al., 2006, Ibanez et al., 2007) a regional stress field (with a NW-SE principal stress direction as σ1) is added as a pre-existing stress field on the stress modelling. Based on the seismic tensor inversion and GPS data, the inferred stress field and maximum horizontal stress for Al-Hoceima – Alboran region is in good agreement with convergence models along the plate boundary (Demets et al., 2010; Meghraoui and Pondrelli, 2012). Note that the magnitude of the principal pre-existing stresses does not change the static coulomb stress modelling, because the stress levels are largely dominated by the coseismic rupture process in the near field.

At seismogenic depth and for optimal failure planes, The static stress change modelling due to the 2004 earthquake on optimally oriented fault planes suggest that ~30 %

of aftershocks hypocentres were pushed closer to failure for high effective friction coefficients (Figure S2 c and d), while this percentage rises to ~90% when pore fluid are redistributed (Figure S 2 a and b)

The elastic modelling in Figure 3a represent the stress change caused by the 1994 earthquake along the 2004 fault zone (with strike-slip mechanism, see also Table 3). The ΔCFF profile are constrained by the aftershock distributions and the computation is performed for receiver faults with strike/dip/rake = 340°/87°/-161°. For the modelling procedure we assume a 0.25 typical value of Poisson ratio with 8×10^5 bar for the Young modulus and $3.3.\times 10^5$ bar for the shear modulus in the seismogenic layer (5 – 15 km thickness). Here, the ΔCFF modelling require a low effective friction coefficient ($\mu' \leq 0.4$) denoting a pore fluid effect. At the 2004 epicentre area, the modelling suggest that the rupture nucleation occurs when pore fluids are redistributed, with the $\mu' \leq 0.4$ considered as an optimal value also explains the nucleation process for a chosen receiver fault geometry. The increase of pore pressure may trigger seismic events in regions where reduced Coulomb stress due to the high effective friction coefficient predict and absence of activity (see also Figure S 2). In fact, the low friction coefficient implies an optimum value of stress loading where the pore fluid component takes an important role in stress transfer and earthquake triggering. The earthquake triggering caused by the 1994 seismic event results from 0.1 – 1.0 bar ΔCFF at the 2016 and 2004 receiver faults, respectively (Figure 3a; Table 3). The ΔCFF modelling shows that the stress transfer due to the 1994 earthquake promotes the 2004 earthquake failure (Figure 2-a, Figure 3, Table3 and Figures S1-a), and both 1994 and 2004 earthquakes promote the failure of the 2016 earthquake (Figure 2 a and b, Table 3 and Figure S1-b). The cumulative post-seismic deformation due to the elastic dislocation increases the stress loading on the 2016 rupture from 0.24 to 0.3 bars.

Role of Pore-fluid in the earthquake sequence

A stress change may result from pore fluid diffusion. If the stress field satisfies the strain compatibility equation $\frac{\partial^2}{\partial x_j^2}\left[\frac{2(\nu_u-\nu)}{B(1-\nu)(1+\nu_u)}P+\sigma\right]=0$ (Rice and Cleary., 1976; see also appendix A for more details) and if we consider the boundary condition (pore pressure is neglected far from the fault), a simple solution is given by Bosl and Nur (2002):

$$\frac{\sigma}{\sigma_{init}}=\frac{(\nu_u-\nu)}{(1-\nu)(1+\nu_u)} \quad (6)$$

Where σ is the change in the stress field due to the pore fluid diffusion, σ_{init} is the initial stress induced by the coseismic dislocation, and ν_u and ν are the undrained and drained Poisson ratio, respectively. This relation also shows the correspondence between the postseismic mean stress change induced by pore pressure relaxation and the mean stress caused by the initial dislocation. Taking into account the Rice and Cleary (1976) and Bosl and Nur (2002) solutions, the short-term poro-elastic deformation is defined as a diffusive process and can be interpreted as a linear combination of pore pressure and mean stress changes.

The drained and undrained Poisson ratios used in the coupled poro-elastic stress modelling are 0.25 and 0.31, respectively (Figure 3b); these values are typical in unconsolidated sedimentary aquifers and water saturated rocks in the upper few kilometers of the seismogenic zone (h ≤ 15-km-depth). Our coupled poro-elastic modelling suggest a value of short term postseimic stress equal to 0.6 bar due to the coupled poro-elastic effect for μ' = 0.4 related to a an internal friction coefficient of μ = 0.75 and Skempton coefficient B = 0.47. The μ' < 0.4 effective friction coefficient gives a value of μ = 0.75 and Skempton coefficient B = 0.9. The variation of B at the intersection of the two ruptures to the end of the 2004 rupture zone can be interpreted as a variation of porosity and the diffusive process along the fault zone (Scholz, 1990).

The same phenomenon is observed in reservoir induced seismicity where the elastic and the coupled poro-elastic effects are considered instantaneous (Scholz, 1990). The diffusive process from the reservoir is associated with the fluid migration at short time delay, and moving from a region with a high B to a region with a low B, indicating a short time poro-elastic rebound where the fluid flow transfer from the 1994 and 2004 rupture zones can be compared as reservoir induced seismic activity.

Taking into account the time of occurrence of aftershocks and the short term post seismic stress change induced by the mainshock using the Bosl and Nur hypothesis (2002), we note that the stress load occurring 10 to 100 days after the 2004 mainshock is far more important than the stress load due to the several years of postseismic deformation computed by InSAR time series (PS and SBAS, Cetin, 2015). The comparable computations take into account the 2004 rupture as source fault and 2016 rupture as receiver fault, and the postseismic deformation added as a cumulative moment is incorporated into the elastic dislocation modelling.

Due to the absence of pore pressure in-situ data and difficulty to perform a 3-dimensional model of stress change and related poro-elastic dislocation, we use equations (2) and (6) to evaluate the stress and pore pressure changes related to the Al Hoceima earthquake sequence. The apparent constant friction model (equation 2) and variable (or isotropic) friction model (equation 6 and in appendix B) are considered as parameters able to improve our knowledge on the pore fluid effect in the Al Hoceima-Alboran region. Nevertheless, the isotropic poro-elastic model appears to be the most appropriate for modelling the short-term diffusive process in a complex fault zone.

The low value of μ' (≤ 0.4) at the intersection between the 1994 and the 2004 fault (Figure 4) implies that the first shock reduces the pore pressure along the 1994 rupture while it increases along the 2004 rupture. The low value of μ' implies a high values of stress change due to the short term coupled poro-elastic effect (Figure 3b). Figure 4 shows how the pore pressure can affect the triggered seismicity when hydrological processes are coupled to the rupture process. The large pore pressure change associated with the volumetric strain corresponds to fluid migration close to and from the 1994 rupture to the 2004 rupture zone (Figure 4). Das and Scholz (1981) suggest that the stress effect on the fault might be enhanced as *P* (see equation 1) and restored on the main fault, causing fluids to migrate into the receiver fault. The same observation is also made by Jonsson et al (2003) for the Mw 6.5 June 2000 earthquake of SW Iceland showing an increasing water level change associated with high pore pressure change in unconsolidated sedimentary aquifers. The evaluation of pore pressure change at depth in Figure 4 is resolved for a homogeneous elastic half space using the theory of linear elasticity (Rice and Cleary, 1976); equation 5 (see also appendix A5) is used to evaluate the pore pressure change by computing the mean stress change due to the 1994 earthquake for a constant Skempton coefficient.

The successive earthquakes in the Al Hoceima region may be a response to stress loading in the Rif Mountains and related pore-fluid diffusion in the upper crust. The coupling between crustal deformation and pore-fluid effect imply that the pore pressure may decrease the rock strength by reducing the effective stress and creating a slip-instability that favours earthquake triggering. The seismicity rate change following the 2004 earthquake shows additional aftershocks (see relative rate fluctuations in Figure 5a), which cannot be explained as aftershock rate decrease as predicted by the Omori law. As the afterslip along seismic ruptures and related postseismic deformation (Cetin, 2015) may have enhanced the pore-fluid flow and contributed to the earthquake triggering in the Rif-Alboran region, in our case, we include a coupled poro-elastic component in the ΔCFF modelling and analyse the postseismic stress transfer and related effective friction coefficient ($\mu' \leq 0.4$). The ΔCFF due to the full poro-elastic relaxation is simply computed from a dislocation in a homogeneous elastic half-space using both undrained and drained Poisson's ratios and obtain the difference as seen in Figure S3.

The pore-fluid flow in drained condition should reduce the normal stress σ_n (equation 2) and favour significant additional aftershocks able to affect the relative seismicity rate change (Nur and Booker, 1972; Cocco and Rice, 2002). In our case, the deep-seated water flow in the flysch units of the fold-and-thrust Rif Belt and substratum metamorphic complex (Chalouan et al., 2008) can be considered as another mechanism responsible for the seismicity increase. Piombo et al. (2005) suggest that for significant earthquakes with Mw > 6, the stress transfer may occur under a fluid diffusion within a 10 to 20 km radius. The temporal evolution of seismicity within individual fractures takes 10-12 years to travel up to 20km (5-6 km per year) in our case as well as in other case studies (e.g., Pytharouli et al., 2011).

Taking into account the complexity of aftershock sequences, a realistic representation of the temporal postseismic factor, the modified Omori Law (Utsu, 1969) or Omori-Utsu Law (Narteau et al, 2009) can be expressed as :

$$\lambda\,(t) = \frac{k}{(t+c)^{-x}} \qquad (7)$$

where λ is the aftershock frequency within a given magnitude range, *t* is the time from the mainshock triggered event, *k* is the productivity of aftershocks that depends on the total number of events, *x* is the power law exponent, and *c* the time delay before the onset of the power-law aftershock decay rate and is dependent on the rate of activity in the earlier part of the seismic sequence. The change of *c* values characterises the aftershocks sequence and can be correlated with the stress field orientation (Narteau et al., 2009), Guo and Ogata (1997) obtain a range of c value between 0.003-0.3 days for various earthquake datasets. In our case, the *c* value has to be the lowest possible and is fixed as 0.01 days, in order to obtain sufficient aftershock productivity. Note that the c value is often retained connected to the incompleteness of seismic catalogues soon after strong earthquakes.

For aftershocks, the seismicity decay requires a time-dependent process that is much faster than the large scale tectonic loading and much slower than the propagation of elastic waves (Nur and Booker, 1972). In our application, we observe that immediately after the 2004 mainshock, the aftershock rate decays by $\frac{1}{\sqrt{t}}$ while it becomes equal to $\frac{1}{t}$ in subsequent months. It appears that the decay rate is due to fluid flow in the crust by means of a diffusion process that contributes to the aftershock sequence (Figure 5 b). Similar results are obtained by Shapiro el al (1997) for the events related to pressure changes in operation wells and recently by Turkaya et al (2015) in laboratory experiments.

The clock time advance and periodic frequency

The Al Hoceima earthquake sequence shows about 10 and 12 years recurrence with an aftershock distribution and stress loading that correlate with the location of earthquake ruptures (Figures 2d, S2a and S3). The mechanism controlling the dependence time of earthquake ruptures, aftershocks and related stress change is complex. The well resolved 2004 aftershocks distribution during a short time interval (100 days; Tahayt et al., 2009) confirms our observation that a significant seismicity rate change is observed 50 days after the mainshocks (see Figure 5 a); the positive change in seismicity is correlated with the positive aftershocks productivity due to pore fluid diffusivity (Figure 5b).

To study the influence of the coseismic stress change on recurrence time interval Chéry et al. (2001) point that a positive shear stress change on a fault plane should advance the time of the next earthquake on this fault. Here we consider that the nucleation will occur where the ΔCFF has a maximum value (Console et al., 2010). The clock time advance and related recurrence time (in years) depends on the stressing rate in the positive ΔCFF expressed by the linear equation (Stein et al., 1997):

$$Tr' = Tr - \Delta CFF/\dot{\tau}, \qquad (8)$$

Where Tr' is the calculated recurrence time, $\Delta t = \Delta CFF/\dot{\tau}$ is the clock time advance ($\dot{\boldsymbol{\tau}}$ is stressing rate), and Tr is the mean recurrence time before the earthquake. The stressing rate is computed from the strain rate which is derived from the seismic moment following the equation: $\dot{M} = 2\mu\Sigma W\dot{\varepsilon}/k$ where μ is the shear modulus, Σ is the surface area of the region, W is the seismogenic thickness, $\dot{\varepsilon}$ is the strain rate and parameter k is a dimensionless constant that adjusts for the inefficiency of randomly oriented faults to accommodate strain. Note that Kostrov (1974) chooses k =1, while Anderson (1979) chooses k =0.75, and using their relations, our calculated strain rate gives 19 and 24 nanostrain/year, respectively (see Table 4). These strain rate values are comparable to the Negredo et al. (2002) and Palano et al. (2013) results and stressing rate of 461 Pa/yr and 582 Pa/yr, respectively. Hence, for the 1.1 bar maximum stress change obtained from the Coulomb modelling on the 2004 receiver rupture (Table 3), the clock time advance Δt for the 2004 receiver source able to generate a significant earthquake with Mw ≥ 6 is 239 ± 22 year using the Kostrov (1974) relation and 189 ± 17 year using the Anderson (1979) relation.

From the seismicity catalogue, the conditional probability for a specified time interval depends only on the time interval ΔT, and the long-term regional seismicity rate**.** The conditional probability for earthquake triggering with Mw > 6 for the Al Hoceima region is given by (Cornell, 1968):

$$Pc = 1 - e^{-\lambda \Delta T} \tag{9}$$

Where λ is the seismicity rate with magnitude M > 6, and ΔT, is the elapsed time since the most recent large earthquake (M > 6) obtained from the Moroccan seismicity catalogue (Jabour, personal communication). The value of λ is obtained from the Gutenberg-Richter (G-R) law constrained by the parameters a and b. Here, we also observe that λ is different before and after the 1994 stress perturbation (λ ranges between 0.012 and 0.09 following the 1994 earthquake). Based on Cornell and Winterstein (1988) hypothesis, the conditional probability related to seismic recurrence models appears to be the most appropriate i) where the hazard is dominated by the nearest fault segment, and ii) in the absence of slip rate and strain rate on each fault segment.

We show in Table 4 that after the 1994 earthquake, the 2004 earthquake fault is under a high value of clock time advance, e.g., Δt = 239 ±22 year or Δt = 189 ±17 year according to Kostrov (1974) and Anderson (1979) formula's, respectively. However, the conditional probability for a specified time interval of 10 years to have an earthquake with Mw > 6 rises from 12 % to 55% (from Equation 9, see also Table 4), in agreement with the seismic rate activity. The change in pore-fluid pressure along ruptures induced by successive earthquakes results in a cluster of large seismic events (Mw > 6) during a short period of time (~22 years).

The conditional probability Pc is similar in the 2004 and the 2016 seismogenic area since we consider the regional probability condition. In his study of the 1992 Landers California earthquake (Mw 7.3), Hardebeck (2004) shows no significant difference in the uncertainty between the conditional probability obtained from stress change and that based on the G-R distribution. In our case, Pc depends only on the G-R seismicity temporal distribution, while other studies use different approaches based mainly on stress drop.

Discussion and conclusion

A sequence of three earthquakes occurred in the Rif Mountains and nearby Alboran Sea in 1994 (Mw 6.0), 2004 (Mw 6.4) and 2016 (Mw 6.5). The static stress change modelling (ΔCFF in undrained condition) suggest a fault rupture interaction with stress loading located on the selected receiver faults. The poro-elastic relaxation (drained condition) and the coupled short term poro-elastic stress transfer help us to understand the seismic migration induced by the pore-fluid diffusion. Aftershock sequences of the three earthquakes correlate well with the

ΔCFF distribution which confirms the role of pore fluid in the triggering of post-1994 earthquakes (Figures S2 and S3). Besides the fault rupture complexity, the modelling parameters require two levels of friction coefficient with μ' < 0.4 correlating with significant pore-fluid diffusivity, and μ' = 0.4 in fault zones with limited diffusivity (Figure 3b). The stress change and related pore-fluid diffusion may explain the ~10-12 years interval and the seismic sequence migration. The role of strain rate and its impact on stress change and pore-fluid diffusion combined with the permeability along fault-rupture zones in the Al Hoceima region is crucial in the comprehension of the time delay between the earthquake sequences.

The 1994 and the 2004 earthquake ruptures illustrate the stress level change, related value of friction coefficient and role of pore-fluid diffusion in conjugate fault geometry. Although the accuracy in location of the 1994 and 2016 aftershocks is limited due to the azimuthal gap and absence of near field seismic stations, the distribution of seismic sequences concurs with the ΔCFF and cumulative loading areas (Figure S3). However, the incomplete seismicity catalogue with precise earthquake locations in the Al Hoceima region prevents a suitable study on the role of fluid pore-pressure before the 1994 earthquake sequence.

The earthquake fault locations inland retrieved from the InSAR analysis of coseismic and after slip surface deformation agree with the aftershock distribution. The limited distance between earthquake ruptures (< 25 km) and fault geometries with strike-slip mechanisms also promote the stress transfer and failure on fixed fault planes. Earthquake faults in the Al Hoceima region are blind with basically no geomorphological signature at the surface (Tahayt et al., 2009). Therefore, fault parameters such as slip-per-event; long-term active deformation and slip rate are missing in our study.

The static strain release by the 1994 event induced a high pore pressure change with fluid flow on the 2004 rupture area. This hydrological phenomenon affects the fault zone permeability and promotes the failure of the 2004 event. Wang (2010) uses the correlation between fluid migration and rock permeability (Rojstascer et al., 2008) to explain the link between the two phenomena; he points out that if the pore pressure becomes too large, earthquakes occur and will increase permeability with groundwater fluid flow.

For a strain rate ranging between 19 and 24 nanostrain/yr. (Table 4), we observe that the regional aftershock frequency following the 2004 earthquake (Figure 5b) is in good agreement with the simulated aftershock frequency based on the pore fluid diffusion hypothesis (Bosl and Nur, 2002). Pore-fluid effects comparable to our case study at the intersection between the 1994 and 2004 ruptures (Figure 4) are also observed for conjugate earthquake ruptures during the Superstition Hills earthquakes (Hudnut et al., 1989, Scholz, 1990). In addition, the decay in the 2004 aftershock activity includes variable seismicity rate probably due to the pore fluid diffusion. A similar behaviour is observed during the 1966 Parkfield-Cholame earthquake where aftershock productivity and related fluid pore-pressure have a direct effect on rock strength (Nur and Booker, 1972).

Depending on the geological structures, substratum permeability and seismicity rate, the 2004 and 2016 earthquakes could have been predictable by the Coulomb modelling taking into account the pore-fluid effect (undrained and drained conditions). In fact, the occurrence of the 21 January 2016 Mw 5.0 foreshock (4 days before the mainshock) may have allowed the fluids to migrate across the epicentral area promoting the 2016 earthquake rupture. Comparable phenomenon with foreshocks and fluid migration across a fault zone is described for the L'Aquila earthquake sequence (Lucente et al, 2010).

The time-scale of post-stress redistribution for the 1994, 2004 and 2016 Al Hoceima earthquakes is larger, for instance, than the ~11 hour Superstitions Hills sequences (Mw 6.2 and 6.6), suggesting different diffusion processes probably controlled by the permeability along the fault zone. Following the 1994 earthquake sequence, the probability for triggering an Mw > 6 earthquake within 10 years interval increases to 55% with respect to the 12% pre-

1994 period (Table 4). With the computed 239 ±22 years clock time advance for large earthquakes (Mw > 6) on the 2004 rupture, the seismic strain rate and ΔCFF explains the 10 – 12 years delay and the 55 % probability of promoting failure in the Rif Mountains.

Acknowledgements: K. J. benefits from a scholarship from the Algerian Ministry of Higher Education and Scientific Research (MESRS). The authors wish to thank Nacer Jabour (CNRST Rabat) and Abdelilah Tahayt (University Mohamed V, Rabat) for the access to the seismicity database. We are thankful to Zoe Shipton and Mark Stillings for reading an early version of the manuscript, and to Ross Stein and Shinji Toda for sharing the Coulomb 3.4 software. We are grateful to two anonymous reviewers for their comments on an early version of the manuscript. This research program was funded by the Direction of Research at MESRS and the DERCI-CNRS with INSU-UMR 7516 IPG Strasbourg. Some figures were prepared using the public domain GMT software (Wessel and Smith, 1998).

References

Akoglu, A. M., Cakir, Z., Meghraoui, M., Belabbes, S., El Alami, S.O, Ergintav, S. & Akyüz, H.S., 2006. The 1994–2004 Al Hoceima (Morocco) earthquake sequence: Conjugate fault ruptures deduced from InSAR, *Earth Planet. Sci. Lett.*, 252, 467–480.

Anderson, J. G., 1979. Estimating the seismicity from geological structure for seismic-risk studies, *Bull. Seism. Soc. Am.*, 69,135–158

Beeler, N.M., Simpson, R.W., Hickman, S.H. & Lockner, D.A., 2000. Pore fluid pressure, apparent friction, and Coulomb failure, *J. Geophys. Res.*, 105, B11, P 25,533-25,542.

Bezzeghoud, M. & Buforn, E., 1999. Source parameters of the 1992 Melilla (Spain, Mw = 4.8), 1994 Al Hoceima (Morocco Mw = 5. 8) and Mascara (Algeria, Mw 5.7) earthquakes and seismotectonic implications, *Bull. Seismol. Soc. Am.*, 89, 359–372.

Biggs, J., Bergman, E., Emmerson, B., Funning, G.J., Jackson, J., Parson, B. & Wright, T.J., 2006. Fault identification for buried strike-slip earthquake using InSAR: The 1994 and 2004 Al Hoceima, Morocco earthquakes, *Geophys. J. Int*, 166, 1347-1362.

Bosl W.J. & Nur, A., 2002. Aftershocks and pore fluid diffusion following the 1992 Landers earthquake, *J. Geophys. Res.*, 107, B12, 2366, doi:10.1029/2001JB000155.

Cakir, Z., Meghraoui, M., Akoglu, A.M., Jabour, N., Belabbes, S. & L. Ait-Brahim, 2006. Surface deformation associated with the Mw 6.4, February 24, 2004 Al Hoceima (Morocco) earthquake deduced from InSAR: implications for the active tectonics along North Africa, *Bull. Seismol. Soc. Am.*, 96 1–10, doi:10.1785/0120050108.

Calvert, A., Gómez, F., Seber, D., Barazangi, M., Jabour, N., Ibenbrahim, A. & Demnati, A., 1997. An integrated geophysical investigation of recent seismicity in the Al-Hoceima region of North Morocco, *Bull. Seismol. Soc. Am.*, 87, 637–651.

Cetin, E., 2015. Analysis and modeling of crustal deformation using InSAR time series along selected active faults within the Africa-Eurasia convergence zone, Ph.D thesis dissertation, University of Strasbourg, EOST, 135 pp.

Chalouan, A., Michard, A., El Kadiri, Kh., Negro, F., Frizon de Lamotte, D., Soto, J.I. & Saddiqi, O., 2008. The Rif Belt, in Continental Evolution: The Geology of Morocco, edited by A. Michard et al., 203–302, Springer, Berlin.

Chéry J., Merkel, S. & Bouissou, S., 2001. A physical basis for time clustering of large earthquakes, *Bull. Seismol. Soc. Am.*, 91, 6, 1685-1693.

Cocco, M. & Rice, J.R., 2003. Pore pressure and poro-elasticity effects in Coulomb stress analysis of earthquake interactions, *J. Geophys. Res.*, **107,** doi:10.1029/2000JB000138 .

Console, R., Murru, M., & G. Falcone, 2010. Probability gains of an epidemic-type aftershock sequence model in retrospective forecasting of M ≥ 5 earth-quakes in Italy, *J. Seismol.*,14,9– 26, doi:10.1007/s10950-009-9161-3.

Cornell, C.A., 1968. Engineering seismic risk analysis, *Bull. Seismol. Soc. Am.*, 58, 1583–1606.

Cornell, C.A. & Winterstein, S.R., 1988. Temporal and magnitude dependence in earthquake recurrence models, *Bull. Seism. Soc. Amer.*, 78, 4, 1522-1573.

Das, S. & Scholz, C.H., 1981. Theory of time-dependent rupture in the Earth, *J. Geophys. Res.*, 86, B7, 6039-6051.

Demets, C., Gordon, R.G., & Argus, D.F., 2010. Geologically current plate motions, *Geophys. J. Int.*, 181, 1-80.

El Alami, S.O., Tadili, B.A., Cherkaoui, T.E., Medina, F., Ramdani, M., Ait Brahim, L., & Harnaff, M., 1998. The Al Hoceima earthquake of May 26, 1994 and its aftershocks: a seismotectonic study, *Ann. Geofis.*, 41, 519–537.

Grevemeyer, I., Gràcia, E., Villaseñor, A., Leuchters, W. & Watts, A.B., 2015. Seismicity and active tectonics in the Alboran Sea, Western Mediterranean: Constraints from an offshore-onshore seismological network and swath bathymetry data, *J. Geophys. Res.*, 120, doi:10.1002/2015JB012073.

Guo., Z. & Ogata, Y., 1997. Statistical relations between the parameters of aftershocks in time, space, and magnitude, *J. Geophys. Res.*, 102, B2, 2857-2873.

Hudnut, W., Seeber, L. & Pacheco, J., 1989. Cross-fault triggering in the November 1987 Superstition Hills earthquake sequence, Southern California, *Geophys. Res. Letters*, Vol. 16, No. 2, 199-202.

Jonsson, S., Segall, P., Pedersen, R. & Bjornsson G., 2003. Post-earthquake ground movements correlated to pore-pressure transients, *Nature*, 424, 179-183.

Kirkpatrick, J. D., Shipton, Z. K., Evans, J. P., Micklethwaite, S., Lim, S. J. & McKillop, P., (2008). Strike-slip fault terminations at seismogenic depths: The structure and kinematics of the Glacier Lakes fault, Sierra Nevada United States, *J. Geophys. Res.*, 113, B04304, doi:10.1029/2007JB005311.

King G.C.P., Stein .R.S & Lin J., 1994. Static stress changes and the triggering of earthquakes, *Bull. Seismol. Soc. Am*, 84, 3, 935-953.

Koulali, A., Ouazar, D., Tahayt, A., King, R.W., Vernant, P., Reilinger, R.E., McClusky, S., Mourabit, T., Davila, J.M. & Amraoui, N., 2011. New GPS constraints on active deformation along the Africa-Iberia plate boundary, *Earth Planet. Sci. Lett.*, 308, 211–217, doi:10.1016/j.epsl.2011.05.048.

Kostrov, V.V., 1974. Seismic moment and energy of earthquakes, and seismic flow of rocks, *Izv. Acad. Sci. USSR Phys. Solid Earth*, 1, Eng. Transl., 23 –44.

Lucente, F. P., Gori P. D., Margheriti, L., Piccinini, D., Bona, M. D., Chiarabba, C. & Agostinetti, N. P., 2010. Temporal variation of seismic velocity and anisotropy before the 2009 Mw 6.3 L'Aquila earthquake, Italy, *Geology*, 38, 1015–1018, doi: 10.1130/G31463.1

Medina, F., 1995. Present-day state of stress in northern Morocco from focal mechanism analysis, *J. Struct. Geol.*, 17 (7), 1035–1046.

Morel, J-L. & Meghraoui, M., 1996. The Goringe–Alboran–Tell tectonic zone, a transpression system along the Africa–Eurasia plate boundary, *Geology*, 24, 755–758.

Meghraoui, M. & Pondrelli, S., 2012. Active faulting and transpression tectonics along the plate boundary in North Africa, *Ann. Geophys.*, 55(5), 955–967, doi:10.4401/ag-4970.

Narteau, C., Byrdina, S., Shebalin, P. & Schorlemmer, D., 2009. Common dependence on stress for the two fundamental laws of statistical seismology, *Nature*, 462, doi: 10.1038.

Nur, A. & Booker, J.R., 1972. Aftershocks caused by pore fluid flow?, *Science*, 25;175(4024), 885-7.

Okada, Y., 1992. Internal deformation due to shear and tensile faults in a half-space, *Bull. Seism. Soc. Amer.*, 82, 2, 1018-1040.

Palano, M., González, P.J. & Fernández, J.A., 2013. Strain and stress fields along the Gibraltar orogenic arc: constraints on active geodynamics, *Gondwana Research*, 23, 1071 – 1088.

Peltzer, G., Rosen, P., Rogez., F & Hudnut, K., 1996. Postseismic rebound in fault step-over caused by pore fluid flow, *Science,* 273, 1202-1204.

Piombo, A., Martinelli G. & Dragoni, M. 2005. Post-seismic fluid flow and Coulomb stress changes in a poro-elastic medium, *Geophys. J. Int*, **162,** 507–515, doi: 10.1111/j.1365-246X.2005.02673.x

Pytharouli, S. I., Lunn, R. J., Shipton, Z. K., Kirkpatrick, J. D. & do Nascimento, A. F., 2011. Microseismicity illuminates open fractures in the shallow crust, *Geophys. Res. Letters*, 38, L02402, doi:10.1029/2010GL045875.

Reasenberg, P.A & Simpson, R.W. 1992. Response of regional seismicity to the static stress change produced by the Loma Prieta earthquake, *Science*, 255, 1687-1690.

Shapiro, S.A., Huenges, E. & Borm, G., 1997. Estimating the crust permeability from fluid-injection-induced seismic emission at the KTB site, *Geophys. J. Int.*, 131, F15–F18.

Segall, P., 2010. Earthquake and Volcano Deformation, Princeton University Press (USA), pp 456.

Scholz, C. H., 1990. The Mechanics of Earthquakes and Faulting, Cambridge University Press (UK), pp. 439.

Stein, R.S., Barka A. & Dieterich, J.H., 1997. Progressive failure on the North Anatolian fault since 1939 by earthquake stress triggering, *Geophys. J. Int.*, 128, 594–604, doi:10.1111/j.1365-246X.1997.tb05321.x.

Stich, D., Serpelloni, E., Mancilla, F. & Morales, J., 2006. Kinematics of the Iberia-Maghreb plate contact from seismic moment tensors and GPS observations, *Tectonophysics*, 426, 295–317.

Tahayt, A., Feigl, K.L., Mourabit, T., Rigo, A., Reilinger, R., McClusky, S., Fadil, A., Berthier, E., Dorbath, L., Serroukh, M., Gomez, F., & Ben Sari, D., 2009. The Al Hoceima (Morocco) earthquake of 24 February (2004) analysis and interpretation of data from ENVISAT ASAR and SPOT5 validated by ground-based observations, *Remote Sens. Environ.*, 113, 306–316.

Terzaghi, K., 1925. Erdbaumechanik auf Bodenphysikalischer Grundlage. Franz Deuticke, Liepzig-Vienna.

Timoulali., Y., Hahou, Y., Jabour, N., Merrouch, R. & El Kharrim, A., 2014. Main features of the deep structure by local earthquake tomography and active tectonics: case of Rif Mountain (Morocco) and Betic Cordillera (Spain), *J. Seismol.*, DOI 10.1007/s10950-013-9385-0

Toda, S., R. S. Stein, Sevilgen V. & Lin J., 2011. Coulomb 3.3 graphic-rich deformation and stress-change software for earthquake, tectonic, and volcano research and teaching, User guide, U.S. Geol. Surv. Open-File Rept. 2011-1060, 63 pp., available at http://pubs.usgs.gov/of/2011/1060/ (last accessed October 2016).

Turkaya, S., Toussaint, R., Ericksen, F.K., Zecevic, M., Daniel, G., Flekkøy, E.G & Måløy, M., 2015. Bridging aero-fracture evolution with the characteristics of the acoustic emissions in a porous medium, *Frontiers in Physics*, 3, doi: 10.3389/fphy.2015.00070.

592 Utsu, T., 1969. Aftershocks and earthquake statistics (I) - Some parameters which characterize an aftershock sequence and their interrelations, *J. Fac. Sci. Hokkaido Univ., Ser.*, VII, 3, 121-195.

595 Vallée, M., Automatic determination of source parameters using the SCARDEC method, http://geoscope.ipgp.fr/index.php/en/catalog/earthquake-description?seis=us10004gy9, (last visit 22 September 2016).

598 Wang C. & Manga, M., 2009. Earthquake and water, Lecture Notes in Earth Science, Springer-Verlag, 114, DOI: 10.1007/978-3-642-00810-8.

600 Wessel, P. & Smith, W.H.F., 1998. New, improved version of generic mapping tools released, *Eos Trans.* AGU, 79(47), 579.

602 Wyss, M. & Habermann, R.E., 1988. Precursory seismic quiescence, *Pure Appl. Geoph.*, 126, 319–332.

604 Wyss, M. & Wiemer, S., 2000. Change in the probabilities for earthquakes in Southern California due to the Landers M 7.3 earthquake, *Science*, 290, 1334–1338.

Table Captions

Table 1: Physical characteristics of the earthquakes used in this study, HRV designed Harvard solution and CMT designed Centroid Moment Tensor solution (see also Figure 1).

Table 2 : Rupture parameters of significant earthquakes from InSAR results (Akoglu et al., 2006) and source time function (http://geoscope.ipgp.fr/index.php/en/catalog/earthquake-description?seis=us10004gy9) used for the Coulomb stress transfer modelling. Long_c and Lat_c indicate the center of each dislocation.

Table 3 : Shear, Normal and Coulomb Stress Change for the major earthquakes. Fault geometries used in the Coulomb stress modelling are defined in Table 2. SF and RF are the source and receiver faults, respectively.

Table 4: Clock time advance (Δt) associated with the ΔCFF and corresponding strain rate in the vicinity of the 1994 source rupture, and for the 2004 and 2016 receiver faults in the Al Hoceima region. k = 0.75 and 1 are the values used by Kostrov (1974) and Anderson (1979), respectively, to compute the strain rate and the conditional probability Pc is calculated over 10 years for earthquakes with Mw > 6.

Figure captions

Figure 1:

Seismicity of the Al Hoceima region showing the seismic sequence of 26/05/1994 (El Alami et al., 1998), 24/02/2004 (Tahayt et al., 2009) and 25/01/2016 (CSEM, http://www.emsc-csem.org/#2). 1994 aftershocks are in green, the 2004 aftershocks are in blue and 2016 aftershocks are in grey. Focal mechanisms are Harvard – CMT (Table 1). Inset represents the plate boundary in the Alboran Sea with convergence rate in mm/yr. (Koulali et al., 2011).

Figure 2: a) calculated ΔCFF with the 1994 source fault, and related aftershock distribution (see text for explanation) and the 2004 as a receiver fault (strike/dip/rake =340°/87°/-161°), the blue, white and black stars are epicentres of the 1999, 2004 and 2016, respectively (same symbols in figure b, c and d). b) Computed ΔCFF with the 2004 as a source fault and the 2016 as a receiver fault (strike/dip/rake = 195°/78°/19°), and related aftershock distribution (see text for explanation),. c) Computed ΔCFF with the 2016 source fault for fixed planes (strike/dip/rake =195°/78°/19°), and related aftershock distribution (see text for explanation), d) Computed cumulative ΔCFF with the three source faults on a fixed planes (strike/dip/rake =195°/78°/19°), and related aftershock distribution (see text for explanation). 1994 and 2004 mapped fault ruptures are from Akoglu et al. (2006), the 2016 fault rupture model is from M. Vallée (http://geoscope.ipgp.fr/index.php/en/catalog/earthquake-description?seis=us10004gy9).

Figure 3:

a) ΔCFF for various effective friction coefficients (μ') along the 2004 rupture (strike direction) as receiver fault with strike/dip/rake = 340°/87°/-161° at 7km depth. The profiles start at the intersection of the two cross faults and terminate at the end of the aftershock sequence (SE of epicentre area). The increases of pore pressure could trigger events in regions where reduced Coulomb stress predict and absence of activity. We show that at the epicenter area, the rupture nucleation occurs when pore fluids are redistributed, the value of $\mu' \leq 0.4$ seems to be more adaptable for a chosen receiver fault geometry. The computation is based on the effective constant friction model.

b) b) Stress change caused by the 1994 earthquake (source fault) along the 2004 fault zone due to 1) coseismic stress change due to elastic dislocation (red line), and 2) stress change due to the coupled poro-elastic effect (green line). The maximum stress load on the 2004 fault zone are given for an isotropic model when $\mu' < 0.4$ that implies Skempton coefficient B=0.9 near the 1994 rupture and for $\mu' = 0.4$ with $B = 0.47$ far from the 1994 rupture.

Figure 4: Calculated pore-pressure change based on the coseismic volumetric strain and theory of linear poro-elasticity (Rice and Cleary., 1976) following the 1994 earthquake. The 1994 and the 2004 rupture are represented by black lines (see also Figure **2d**). The 1994 co-seismic slip create a high pore pressure zone in the rupture nucleation zone of the next 2004 earthquake, according to Terzaghi (1925) definition of effective stress, the increase in pore pressure diminishes the normal stress acting on the fault and promote the 2004 failure.

Figure 5:

a) The seismic frequency and relative seismicity rate following the 2004 mainshock (blue line) and cumulative number of seismic events (green line). The fluctuation in the seismicity rate change shows additional aftershocks possibly due to pore-fluid diffusion in the upper crust. The relative rate changes are obtained from changes in slop of the cumulative number curve using a Habermann function regardless to the time of greatest change and comparing the rate in the two parts of the period (before and after the division point) by appropriate time windows function (Wyss and Habermann., 1988, Wyss and Viemer., 2000). The time variation function defines the local time variation between the rate before and after.

b) The seismicity rate change versus time in the Al Hoceima region. We show the complexity of aftershocks sequences as a realistic representation of the temporal postseismic effect.

Table 1: Physical characteristics of the earthquakes used in this study, HRV designed Harvard solution and CMT designed Centroid Moment Tensor solution (see also Figure 1).

Earthquake	Long.	Lat.	Mo (10^{18} nm)	Mw	U (m)	L (km)	W (km)	Strike	Dip	Rake
26/05/1994	-3.99	35.28	1.01	6,1	0.8	16	10	17	85	-7
24/02/2004	-3.99	35.142	3.0	6.4	1.0	19	16.5	340	87	-161
25/01/2016	-3.70	35.67	4.69	6.5	0.8	25	13.5	214	78	19

Table 2 : Rupture parameters of significant earthquakes from InSAR results (Akoglu et al., 2006) and source time function (http://geoscope.ipgp.fr/index.php/en/catalog/earthquake-description?seis=us10004gy9) used for the Coulomb stress transfer modelling. Long_c and Lat_c indicate the center of each dislocation.

EQ	**Long_c (°)**	**Lat_c (°)**	**Top-Depth (km)**	**Bot-Depth (km)**	**L (km)**	**W (km)**	**Strike (°)**	**Dip (°)**	**Rev. Slip (m)**	**Right _lat. Slip (m)**	**M_0 (dyne .cm) $*10^{25}$**
1994	-4.01	35.17	1.00	11.00	16.00	10.04	17	85	-0.04	-0.32	1.7
2004	-3.97	35.13	1.00	16.00	20.63	15.02	340	87	-0.22	0.63	6.6
2016	-3.84	35.5	1.00	14.47	28.70	13.50	205	86	0.2	-0.57	7.5

Table 3 : Shear, Normal and Coulomb Stress Change for the major earthquakes. Fault geometries used in the Coulomb stress modelling are defined in Table 2. SF and RF are the source and receiver faults, respectively.

EQ	**Calc_Location**			**Receiver Faults (°)**			**Stress Computation (bar)**		
(SF-RF)	**Long (°)**	**Lat(°)**	**Z(km)**	**Strike**	**Dip**	**Rake**	**Shear**	**Normal**	**Coulomb**
1994(SF)	-4.010	35.166	7.00	**340**	**87**	**-161**	**1.997**	**-8.547**	**-1.422**
2004(RF)	-3.931	35.088	7.00				**0.656**	**1.104**	**1.062**
1994(SF)	-3.987	35.131	7.00	**195**	**78**	**19**	**-8.146**	**-1.227**	**-8.637**
2016(RF)	-3.870	35.429	7.00				**0.093**	**0.048**	**0.112**
2004(SF)	-4.008	35.166	7.00	**195**	**78**	**19**	**-4.594**	**-11.509**	**-9.198**
2016(RF)	-3.870	35.429	7.00				**0.228**	**0.033**	**0.241**

Table 4: Clock time advance (Δt) associated with the ΔCFF and corresponding strain rate in the vicinity of the 1994 source rupture, and for the 2004 and 2016 receiver faults in the Al Hoceima region. k = 0.75 and 1 are the values used by Kostrov (1974) and Anderson (1979), respectively, to compute the strain rate and the conditional probability Pc is calculated over 10 years for earthquakes with Mw > 6.

Seismic Ruptures	Strain rate (nanostrain/year)	$\dot{\tau}$ Stress rate (Pa/year)	ΔCFF_{max} (MPa)	$\Delta t = \frac{\Delta CFF}{\acute{\tau}}$ (year)	Pc no Stress Change (pre-1994)	Pc with Stress Change (post-1994)
2004	19 (k=0.75)	461	0.11	239 ±22	12 %	55%
2004	24 (k=1)	582	0.11	189 ±17		
2016	19 (k=0.75)	461	0.02	21 ±02		
2016	24 (k=1)	582	0.02	17 ±02		

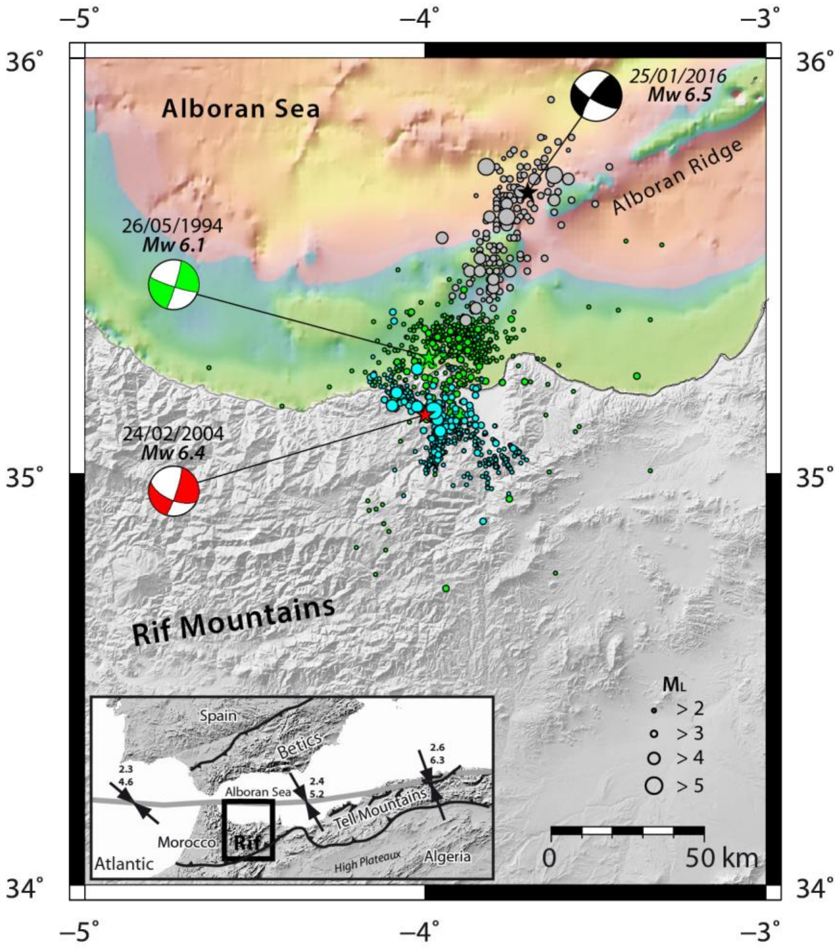

Figure 1:
Seismicity of the Al Hoceima region showing the seismic sequence of 26/05/1994 (El Alami et al., 1998), 24/02/2004 (Tahayt et al., 2009) and 25/01/2016 (CSEM, http://www.emsc-csem.org/#2). 1994 aftershocks are in green, the 2004 aftershocks are in blue and 2016 aftershocks are in grey. Focal mechanisms are Harvard – CMT (Table 1). Inset represents the plate boundary in the Alboran Sea with convergence rate in mm/yr. (Koulali et al., 2011).

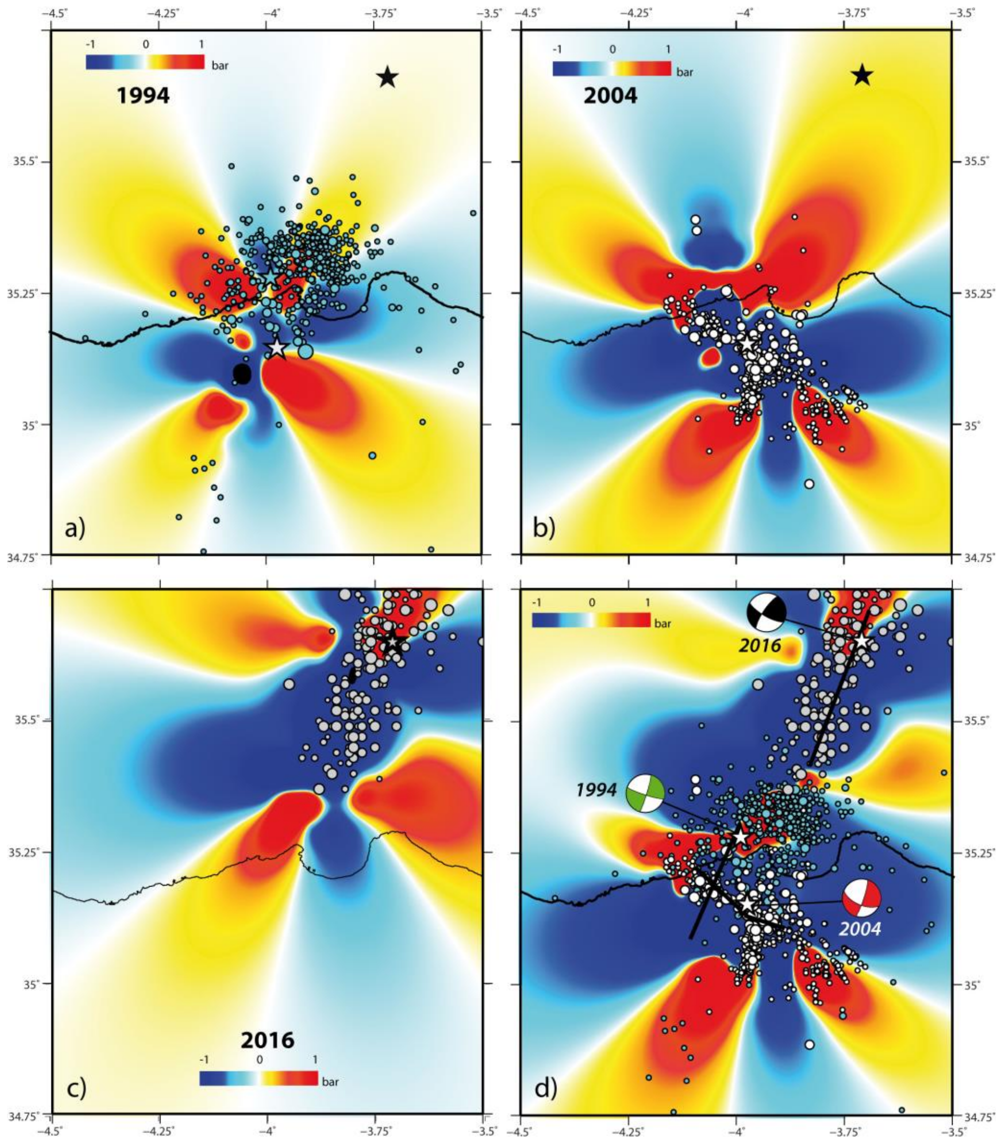

Figure 2: a) calculated ΔCFF with the 1994 source fault, and related aftershock distribution (see text for explanation) and the 2004 as a receiver fault (strike/dip/rake =340°/87°/-161°), the blue, white and black stars are epicentres of the 1999, 2004 and 2016, respectively (same symbols in figure b, c and d). b) Computed ΔCFF with the 2004 as a source fault and the 2016 as a receiver fault (strike/dip/rake = 195°/78°/19°), and related aftershock distribution (see text for explanation),. c) Computed ΔCFF with the 2016 source fault for fixed planes (strike/dip/rake =195°/78°/19°), and related aftershock distribution (see text for explanation), d) Computed cumulative ΔCFF with the three source faults on a fixed planes (strike/dip/rake =195°/78°/19°), and related aftershock distribution (see text for explanation). 1994 and 2004 mapped fault ruptures are from Akoglu et al. (2006), the 2016 fault rupture model is from M. Vallée (http://geoscope.ipgp.fr/index.php/en/catalog/earthquake-description?seis=us10004gy9).

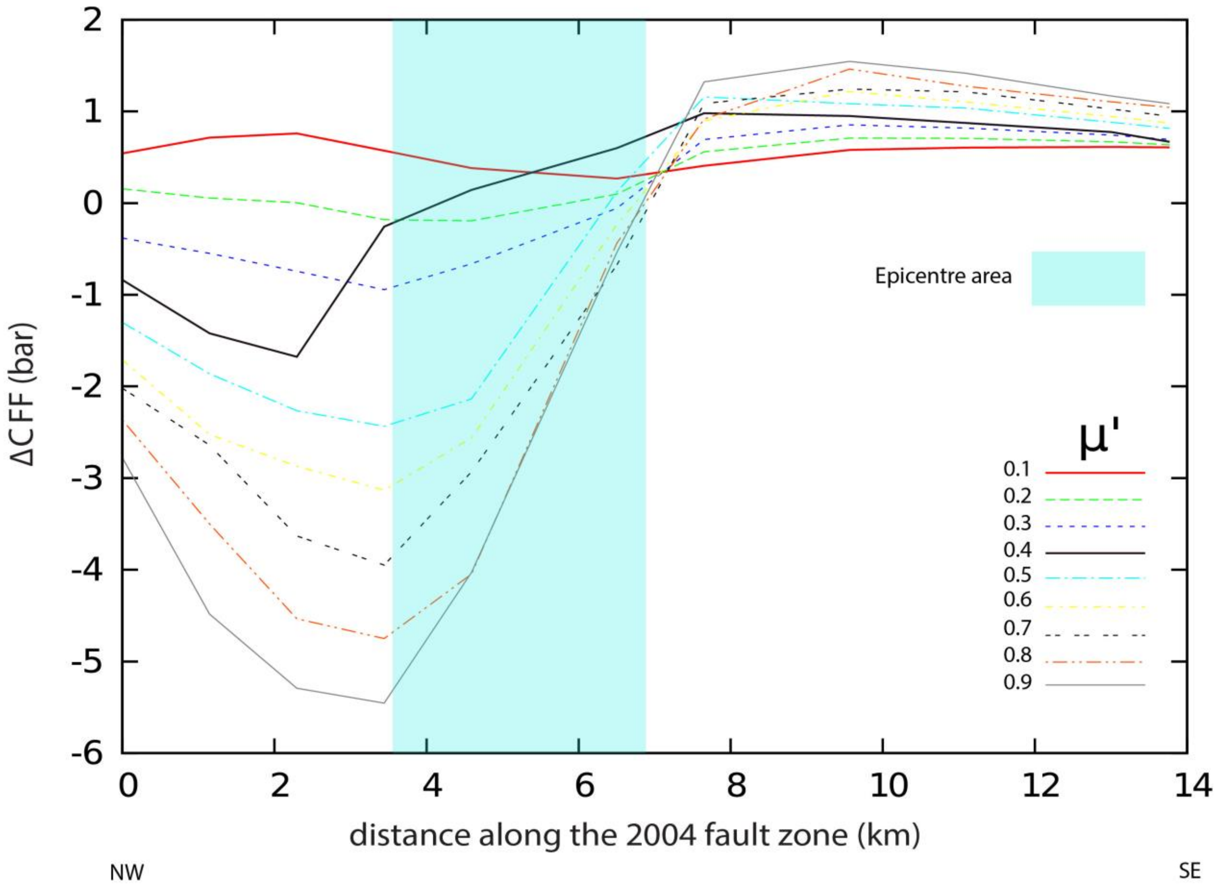

Figure 3: a) ΔCFF for various effective friction coefficients (μ') along the 2004 rupture (strike direction) as receiver fault with strike/dip/rake = 340°/87°/-161° at 7km depth. The profiles start at the intersection of the two cross faults and terminate at the end of the aftershock sequence (SE of epicentre area). The increases of pore pressure could trigger events in regions where reduced Coulomb stress predict and absence of activity. We show that at the epicenter area, the rupture nucleation occurs when pore fluids are redistributed, the value of μ'≤0.4 seems to be more adaptable for a chosen receiver fault geometry. The computation is based on the effective constant friction model.

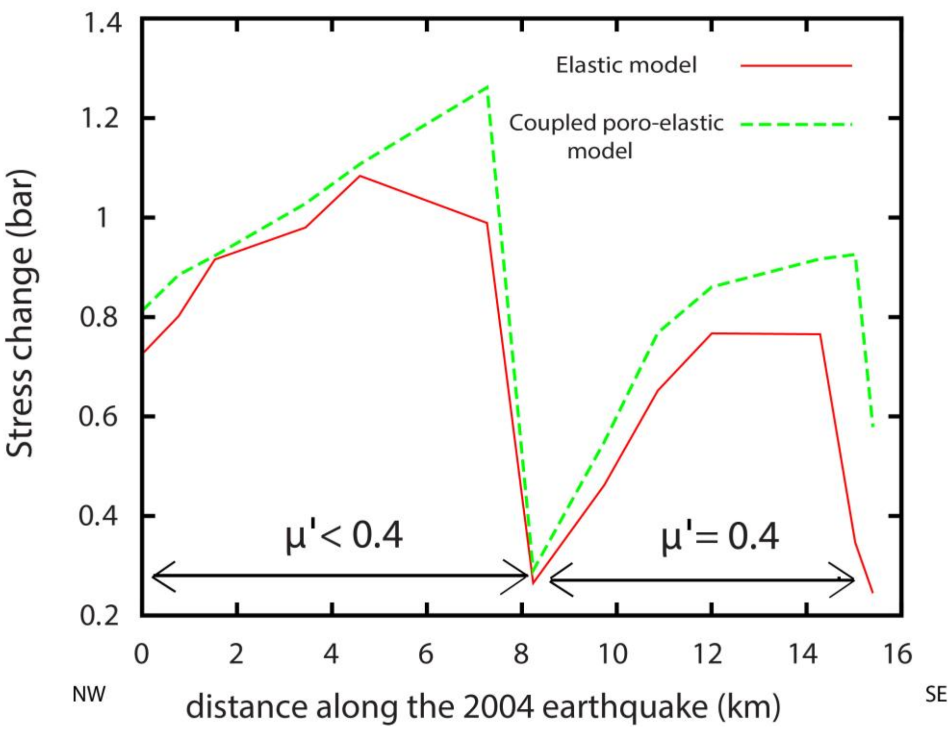

Figure 3: b) Stress change caused by the 1994 earthquake (source fault) along the 2004 fault zone due to 1) coseismic stress change due to elastic dislocation (red line), and 2) stress change due to the coupled poro-elastic effect (green line). The maximum stress load on the 2004 fault zone are given for an isotropic model when μ' < 0.4 that implies Skempton coefficient *B*=0.9 near the 1994 rupture and for μ ' = 0.4 with *B* = 0.47 far from the 1994 rupture.

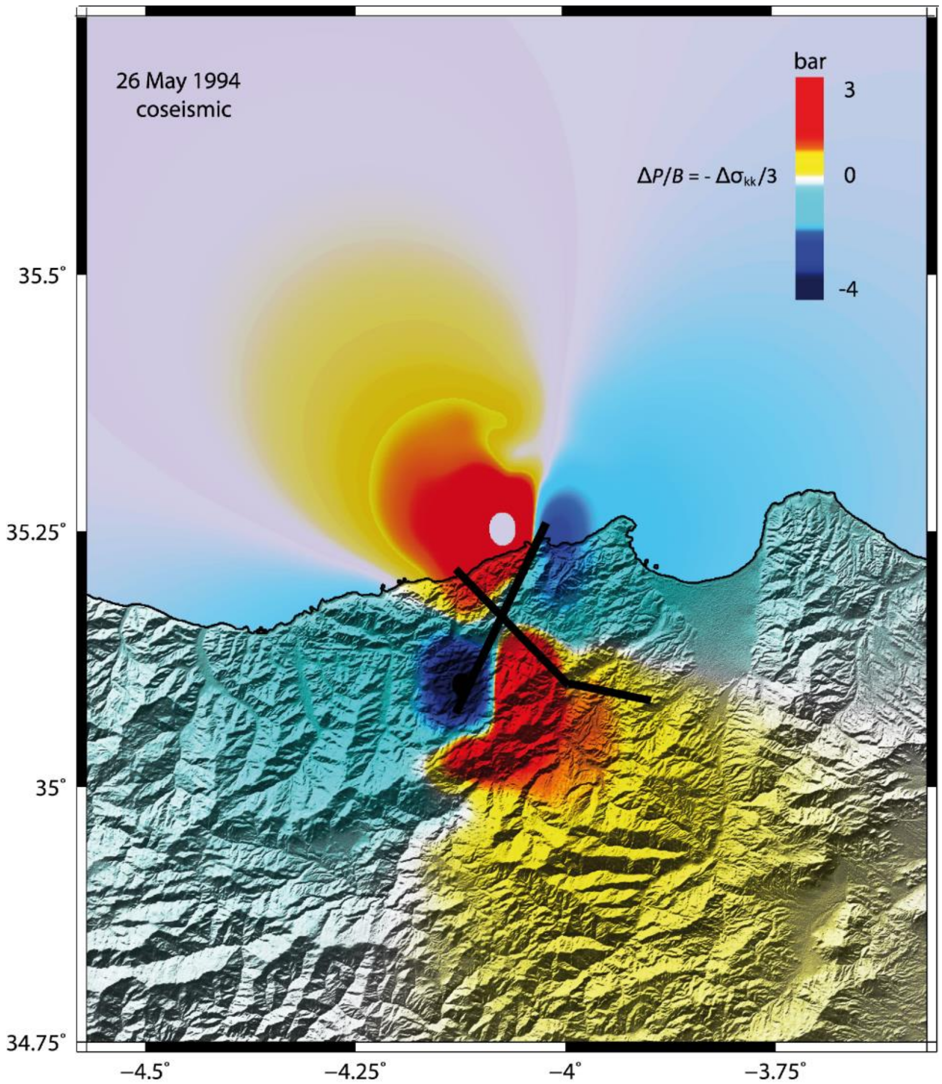

Figure 4: Calculated pore-pressure change based on the coseismic volumetric strain and theory of linear poro-elasticity (Rice and Cleary., 1976) following the 1994 earthquake. The 1994 and the 2004 rupture are represented by black lines (see also Figure **2d**). The 1994 co-seismic slip create a high pore pressure zone in the rupture nucleation zone of the next 2004 earthquake, according to Terzaghi (1925) definition of effective stress, the increase in pore pressure diminishes the normal stress acting on the fault and promote the 2004 failure.

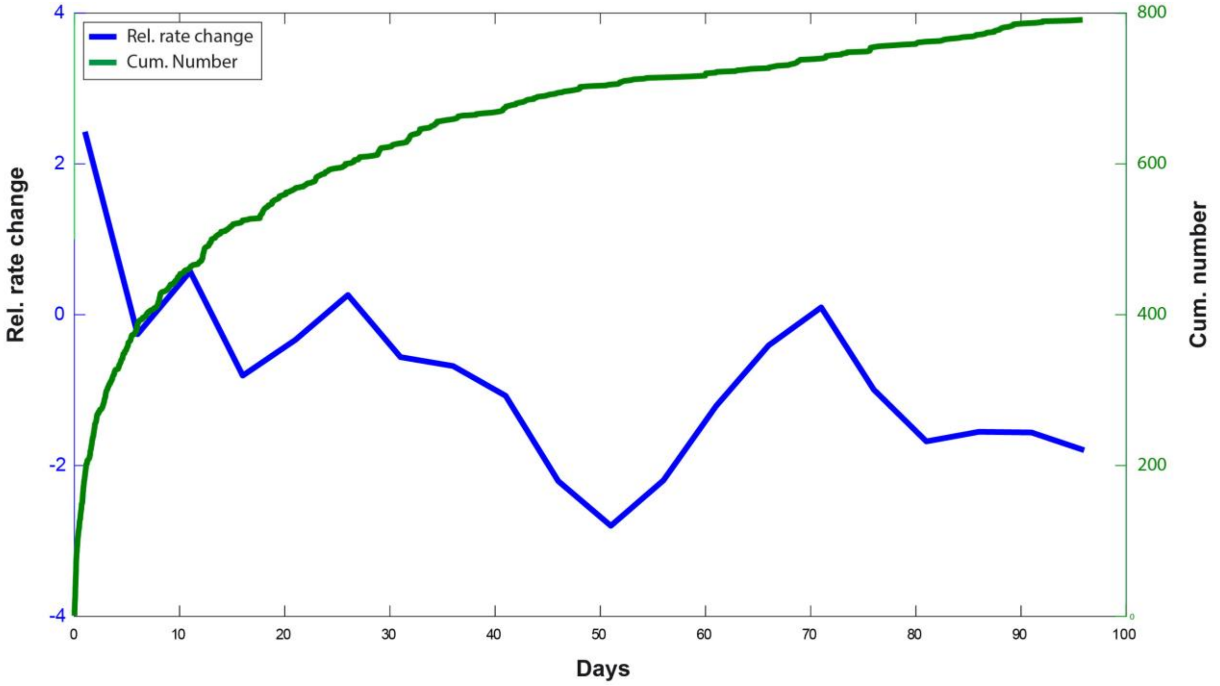

Figure 5: a) The seismic frequency and relative seismicity rate following the 2004 mainshock (blue line) and cumulative number of seismic events (green line). The fluctuation in the seismicity rate change shows additional aftershocks possibly due to pore-fluid diffusion in the upper crust. The relative rate changes are obtained from changes in slop of the cumulative number curve using a Habermann function regardless to the time of greatest change and comparing the rate in the two parts of the period (before and after the division point) by appropriate time windows function (Wyss and Habermann., 1988, Wyss and Viemer., 2000). The time variation function defines the local time variation between the rate before and after.

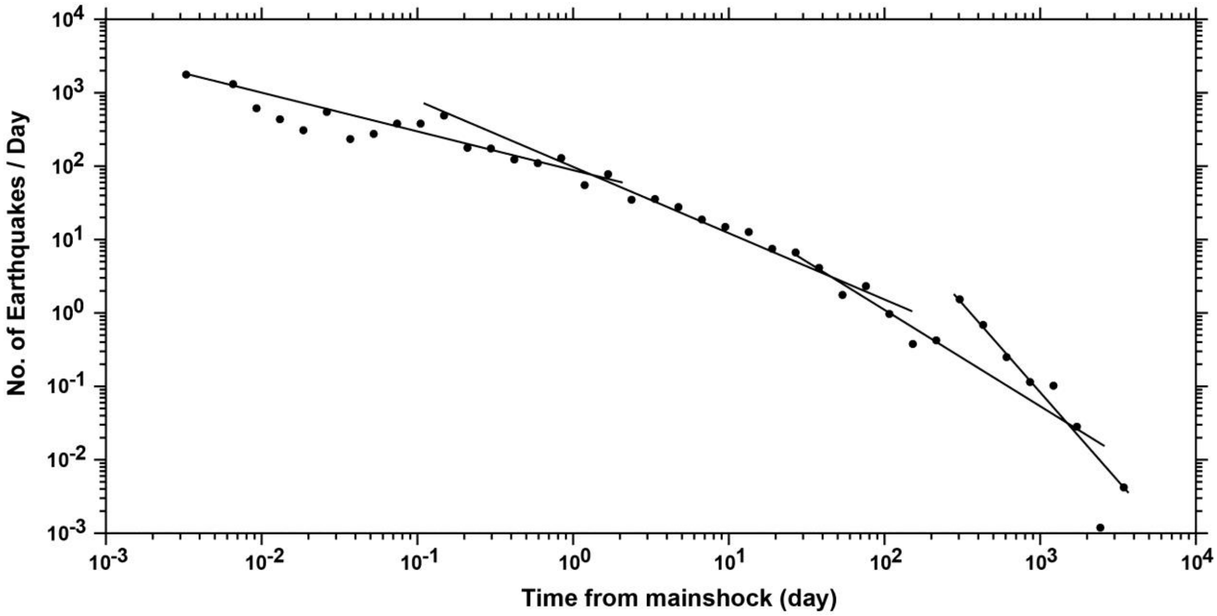

Figure 5: b) The seismicity rate change versus time in the Al Hoceima region. We show the complexity of aftershocks sequences as a realistic representation of the temporal postseismic effect.

Supplemental Material

The Al Hoceima earthquake sequence of 1994, 2004 and 2016: Stress transfer and poro-elasticity in the Rif and Alboran Sea region

J. Kariche, M. Meghraoui, Y. Timoulali,
E. Cetin and R. Toussaint

Figures S1 of the Supplemental Material illustrate the ΔCFF on 2004 and 2016 planes induced by the 1994 and the cumulative 1994 and 2004 respectively. Figure S2 represents the Coulomb stress change computed on optimally oriented fault planes induced by the 2004 rupture, the static stress change are correlated with the seismicity. Figure S3 represents the stress change on the 2004 fault plane due to the full poro-elastic relaxation of the 1994 earthquake using different drained process. Figure S4 shows the angular relationship between stress directions and the 2004 fault plane, this figure as considered as an input to the computation of stress change on the 2004 rupture due to the poro-elastic (or isotropic) model as expressed by Beeler et al (2000).
The Appendix A presents the full constitutive equations used to represent the poro-elasticity at Al Hoceima- Alboran zone. Appendix B details the relationship between the weakness of the Al Hoceima faults system and the stress triggered rely on a fault failure model for an varying effective friction coefficient model, the variable isotropic model are compared to the constant effective friction model in term of stress contribution.

List of Figure Captions

Figure S1: **a)** ΔCFF modelling on the 2004 fault plane due to the 1994 fault rupture, the computation are made for μ’ =0.2, the black stars indicate the 2004 hypocenter, **b)** ΔCFF modelling on the 2016 fault plane due to the cumulative 1994 and 2004 earthquake, the grey stars indicate the 2016 hypocenter, note that the receiver planes are tapered to 40 fault patches system.

Figure S2: ΔCFF modelling on optimally oriented fault planes caused by the 2004 earthquake at depth range [5km-15km] for : **a)** μ’ =0.2, **b)** μ’ =0.4, **c)** μ’ =0.6, **d)** μ’ =0.8, the aftershocks distributions is represented by black circles, the white star represents the 2004 epicenter and the grey star is the 2016 epicenter. The increases of pressure could trigger events in regions where the Coulomb stress predict and absence of activity.

Figure S3: Full poro-elastic relaxation of the 1994 and the 2016 earthquakes from the undrained state to the fully drained state, the computation is obtained by linear elasticity theory with appropriate values of undrained and drained Poisson ratio : **a)** full poro-elastic relaxation due to the 1994 earthquake on the 2004 fault rupture with a typical sedimentary undrained and drained Poisson ratio respectively , **b)** full poro-elastic relaxation due to the 1994 earthquake on the 2004 fault rupture with an extreme undrained and drained Poisson ratio respectively, according the Bosl and Nur hypothesis, this value might be typical for upper crust when fractures exists, **c)** ΔCFF (red + green) and ΔP/B profiles along the 2004 rupture related to the full poro-elastic relaxation of the 1994 earthquake, a significant change of ΔP/B is obtained for $(\nu_u , \nu) = (0.31, 0.15)$, the yellow star indicate the 2004 epicenter location on the axe, **d)** full poro-elastic relaxation due to the 2016 earthquake on fixed planes strike/dip/rake = 195°/78°/19° for $(\nu_u , \nu) = (0.31, 0.15)$, **e)** full poro-elastic relaxation due to the 2016 earthquake on fixed planes strike/dip/rake = 195°/78°/19° for $(\nu_u , \nu) = (0.31, 0.25)$, note that the white stars indicate the 2016 epicenter location.

Figure S4: Angular relationship between preseismic local stress field and the 2004 fault plane acting on the central Rif block, the maximum horizontal stress (green) and the minimum horizontal (yellow) stress directions acting of the 2004 rupture at depth are obtained from stress estimation based on inversion of focal mechanism and GPS data obtained by several authors (Ibanez et al , 2007., Tahayt et al., 2009., Akoglu et al., 2006), σ *and* τ denote the normal and shear stress according to the state of stress, the red black and the red line indicates the SS surface fault of the 1994 and 2004 earthquakes respectively, the tectonic model used for this study are from Tahayt et al (2009) where arrows indicate the relative movements of these blocks with respect to Africa plate, the 1994 and the 2004 rupture are from Akoglu et al (2006). The majors reverse faults trace are represented by an appropriate symbol, the majors strike slip faults trace represented by lines.

Table S: Coulomb stress change caused by the 2004 and the 2016 earthquakes on aftershocks planes for μ' = 0.4, the strike/dip/rake represent the best geometry related to the optimally oriented ΔCFF loading. SF represents the source fault.

Appendix A: Constitutive equations of poro-elasticity.

Appendix B: Relationship between the poro-elastic model and the 2004 earthquake triggering.

Table S1: Coulomb stress change caused by the 2004 and the 2016 earthquakes on aftershocks planes for μ’ = 0.4, the strike/dip/rake represent the best geometry related to the optimally oriented ΔCFF loading. SF represents the source fault.

Source Fault	Year	month	day	hour	min	Long (°)	Lat (°)	Depth (km)	mag	Strike (°)	Dip (°)	Rake (°)	Shear (bar)	Normal (bar)	Coulomb (bar)
2004 SF	**2004**	**02**	**25**	**12**	**44**	**-4.11**	**35.28**	**10.10**	**5.23**	**207**	**66**	**-1**	**0.65**	**1.47**	**0.79**
	2004	**02**	**26**	**12**	**7**	**-4.18**	**35.23**	**10.8**	**4.93**	**298**	**84**	**-154**	**0.45**	**0.04**	**0.45**
	2004	**03**	**7**	**6**	**37**	**-4.02**	**35.04**	**10.00**	**5.05**	**178**	**43**	**-43**	**-0.42**	**0.39**	**-0.38**
	2016	**01**	**25**	**5**	**54**	**-3.77**	**35.48**	**10.00**	**5.38**	**290**	**82**	**-128**	**0.22**	**0.34**	**0.26**
2016 SF	**2016**	**02**	**22**	**3**	**46**	**-3.51**	**35.74**	**10.00**	**5.2**	**252**	**44**	**86**	**0.1**	**-0.01**	**0.1**
	2016	**03**	**11**	**4**	**16**	**-3.60**	**35.70**	**10.00**	**5.0**	**250**	**43**	**85**	**0.18**	**0.02**	**0.2**
	2016	**03**	**15**	**4**	**40**	**-3.63**	**35.69**	**10.00**	**5.3**	**260**	**43**	**95**	**0.4**	**-0.1**	**0.4**

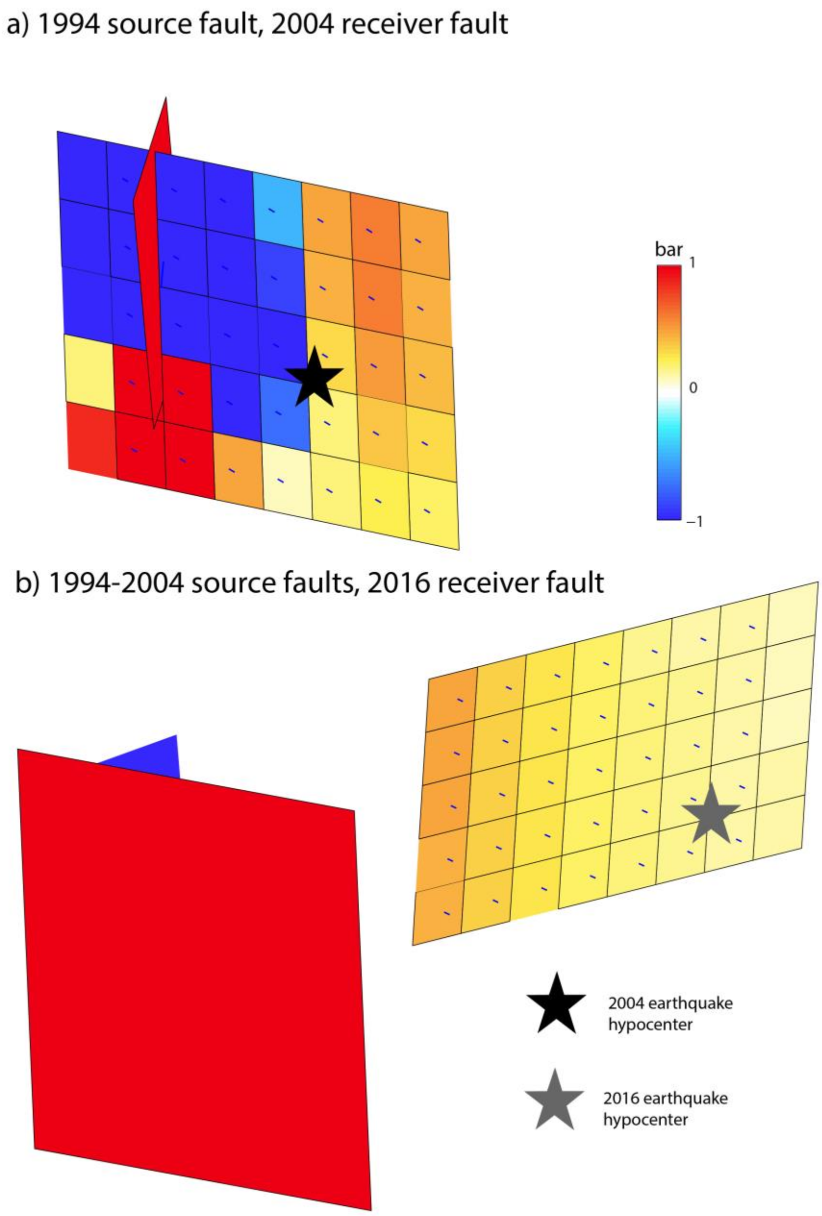

Figures S1 a and b

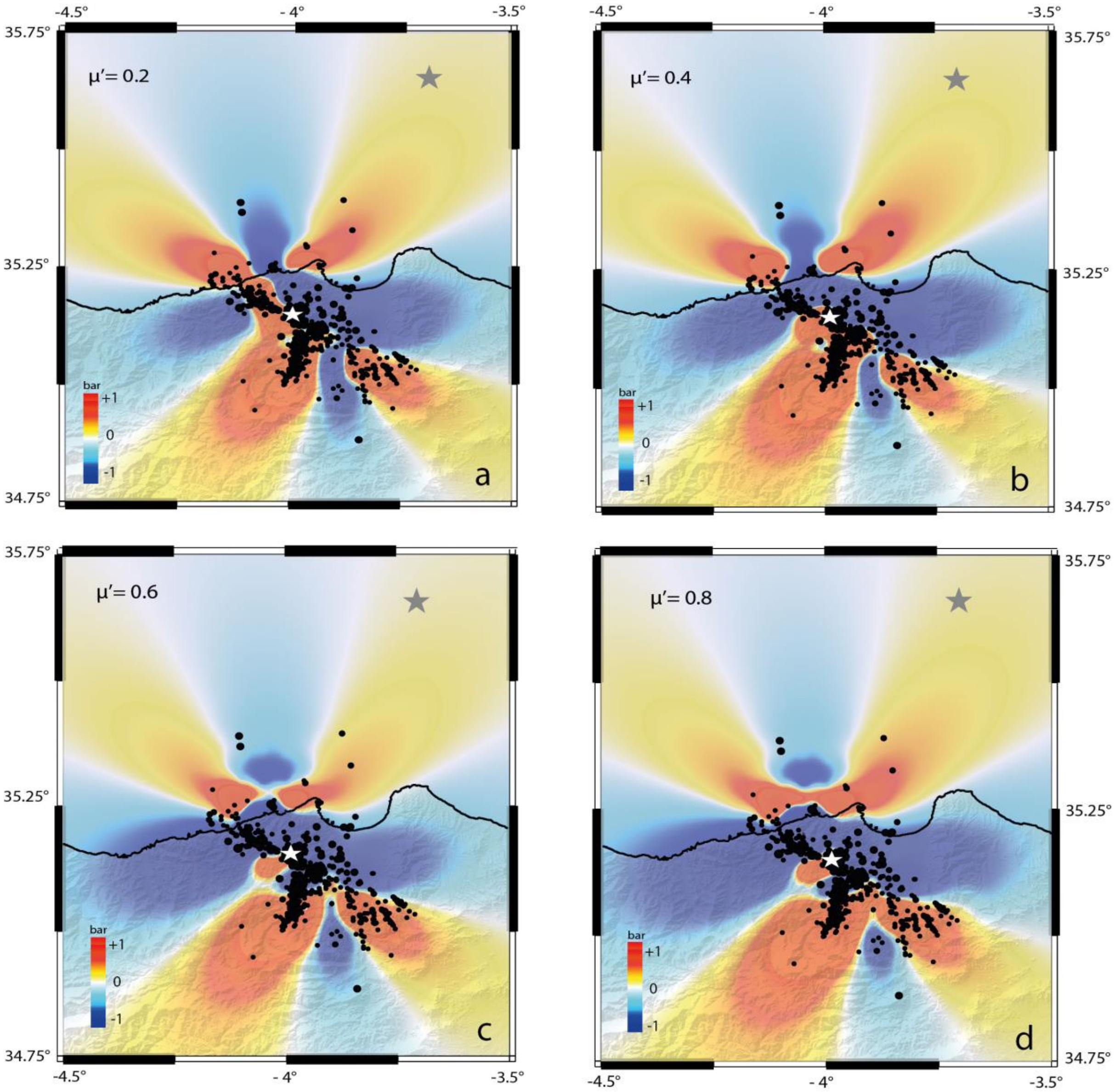

Figures S2 a, b, c and d

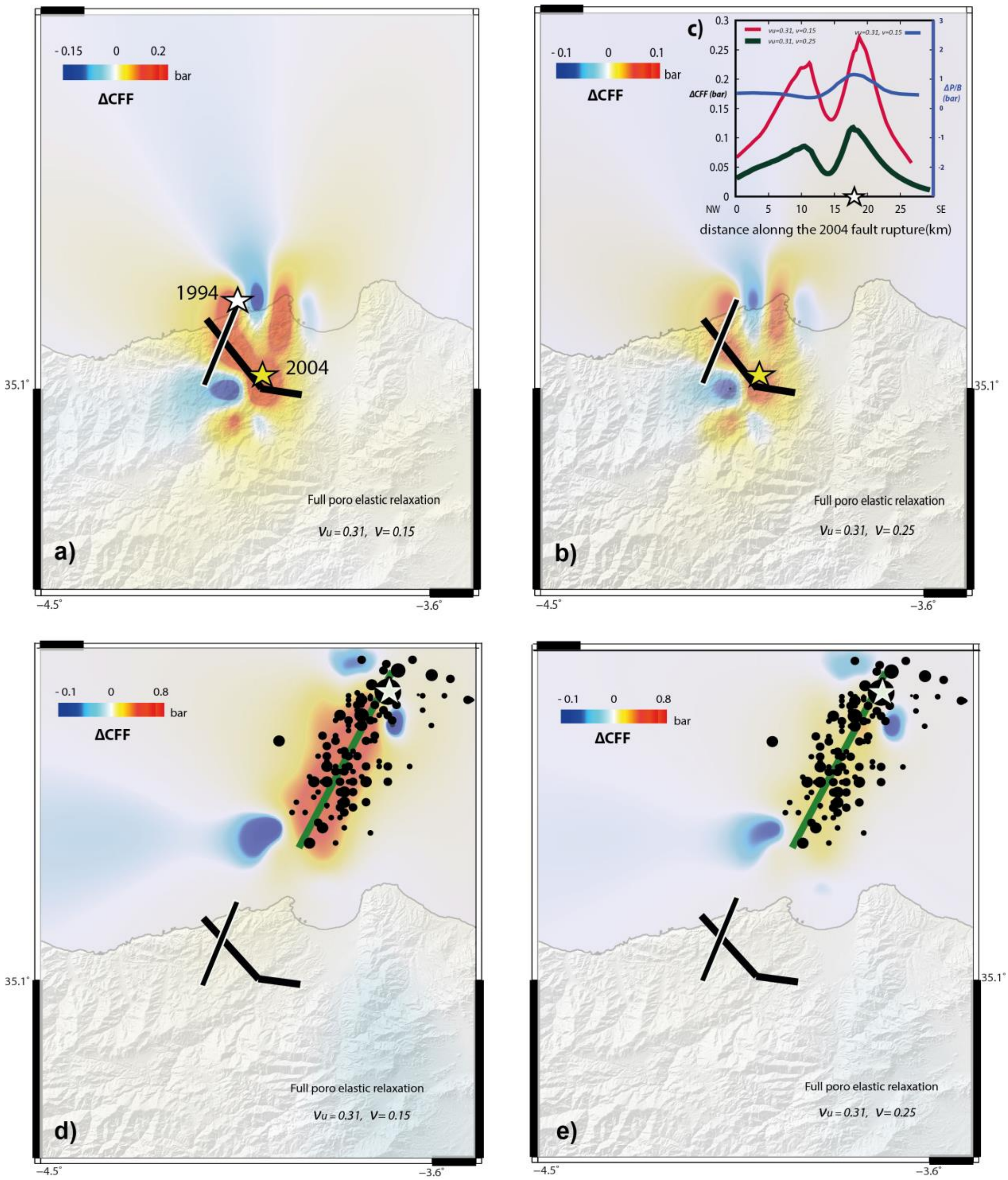

Figures S3 a, b, c, d and e

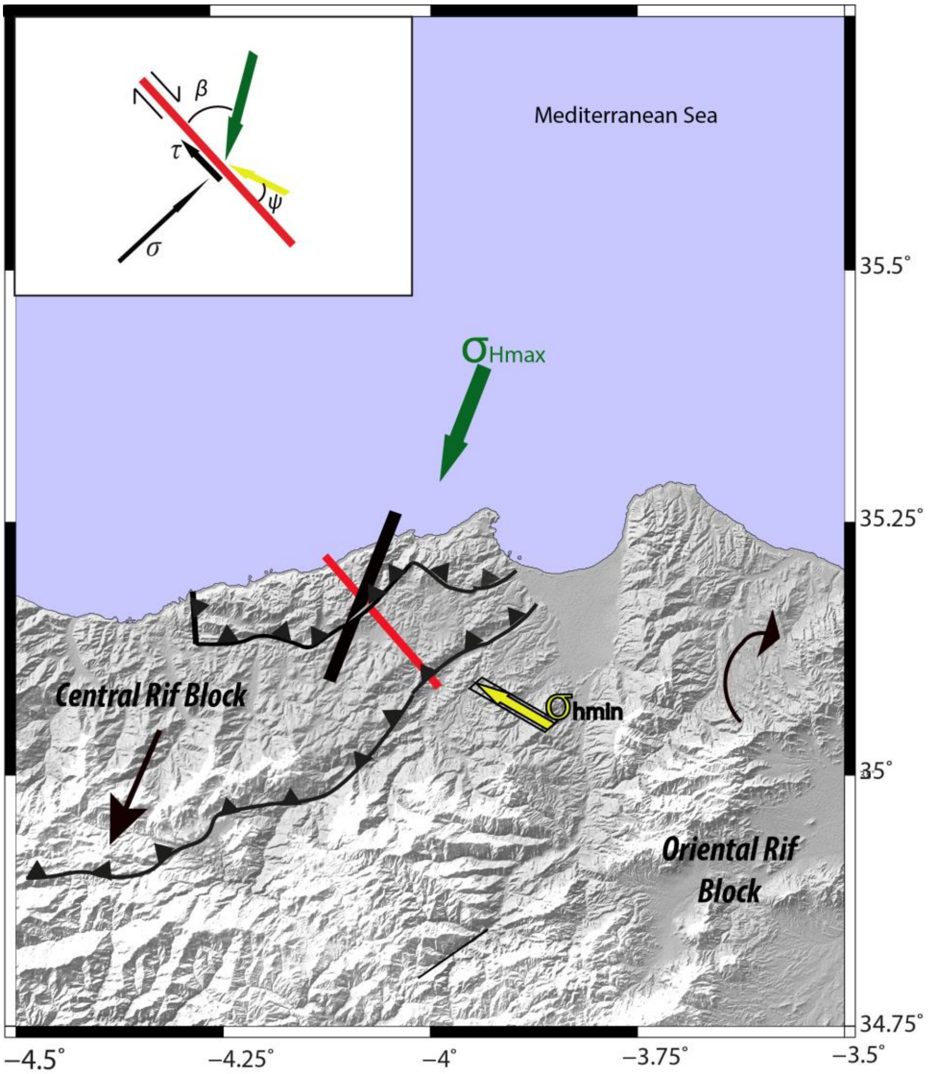
β
τ
ψ
σ
Mediterranean Sea
σHmax
σhmin
Central Rif Block
Oriental Rif Block
35.5°
35.25°
35°
34.75°
−4.5°
−4.25°
−4°
−3.75°
−3.5°

Figure S4

Appendix A: Constitutive equations of poro-elasticity

Based on the fracture mechanical model of fault propagation, Rice and Cleary (1976) rewrite the Biot equations (1941) of linear elasticity takin into account the rupturing solid and its pore fluid component.

In order to solve the equation governing the response to initial stress created by a dislocation in a porous solid, the linearized relation for a fluid saturated porous elastic solid is formulated first by Biot (1941, 1955) who coupled the diffusive aspect of a single phase fluid in a porous medium to the mean stress. The poro-elastic time-dependent equation is formulated in terms of coupled pore pressure and mean stress (Rice and Cleary, 1976; Bosl and Nur, 2002) as following:

$$B\left(\frac{\partial P}{\partial t} + B\frac{\partial \sigma}{\partial t}\right) = \frac{\partial}{\partial x_i}\left(\boldsymbol{k_{ij}}\,(x)\frac{\partial P}{\partial x_j}\right) \qquad (A1)$$

$$B = \mu\, \emptyset\, (C_f + C_r)$$

where μ is the fluid viscosity, $\emptyset$ is the porosity, $C_f\ and\ C_r$ are fluid and rock compressibility respectively, P is the pore deviation from the reference pressure, $\sigma = \frac{\sigma_{kk}}{3}$ is the mean stress deviation from a reference mean stress state ($with\ \sigma = \sigma_{total} - \sigma_{ref}$), B is the Skempton coefficient, and $\boldsymbol{k_{ij}}\,(x)$ is the spatially variable permeability tensor.

The equilibrium equation must be solved from the linear isotropic expression for strain compatibility $(\varepsilon_{ij})\ under\ isotermal$ condition as postulated by Biot (1941) :

$$2G\varepsilon_{IJ} = \left(\sigma_{ij} + P\delta_{ij}\right) - \frac{\nu}{1+\nu}\,(\sigma_{kk} + 3P)\,\sigma_{ij} + \frac{2G}{3}\left(\frac{1}{H} - \frac{1}{K}\right) P\,\sigma_{ij} \qquad (A2)$$

Where H is the poro-elastic expansion coefficient, $\alpha = K/H$ is the Biot-Willis coefficient, G, ν are the shear modulus and poisson ratio, respectively.

Simultaneous change of stress $\Delta\sigma_{ij}$ induced by pore pressure change ΔP is written by Rice and Clearly (1974) as:

$$\Delta\sigma_{ij} = -\Delta P\delta_{ij} \qquad (A3)$$

Where δ_{ij} is a known Kronecker Delta.

The relation that governs the poro-elastic deformation is in the simple form (Rice and Clearly., 1976):

$$\Delta\varepsilon_{ij} = -\,\delta_{ij}\,\frac{\Delta P}{3K_s}\ \ ;\ \ \Delta\nu = -\nu_0\frac{\Delta P}{K_s}$$

The mass equilibrium state is obtained by multiplyingν by ρ, fromA (2):

$$m - m_0 = (\rho - \rho_0)\, v_0 + \rho_0\, (v - v_0)$$
$$= \rho_0 \frac{v_0}{K_f} P + \frac{\rho_0}{3}\left(\frac{1}{K} - \frac{1}{K'_s}\right)(\sigma_{kk} + 3P) - \rho_0 \frac{v_0}{K''_s} P \qquad (A4)$$

m_0 *and* ρ_0 correspond to the reference state and K_f is the Bulk modulus of fluid defined by $\frac{\rho_0 P}{(\rho - \rho_0)}$ and K'_s *and* K''_s can be identified in appropriate circumstances as the bulk modulus K_s of the solid phase (see Rice and Cleary, 1974) and are defined as a local bulk modulus where both fluid and solid are chemically inert. K'_s *and* K''_s are sensibly associated with K_s and must be introduced as experimental constants additional to G and ν and analogous to H *and* R also having the same order of magnitude as the bulk modulus for 'non-fluid-infiltrated' (Rice and Cleary, 1974) .

If we consider that a pore pressure change is induced by an earthquake dislocation, we rewrite equation $(m - m_0)$ at undrained state of deformation, and in this case we assume that the short time scale (coseismic) implies no change in the fluid mass (i.e., Δm = 0). Rice and Cleary (1976) definition of undrained condition is comparable to that stipulated by Bosl and Nur (2002). Based on this assumption, the Rice and Cleary (1974) short term undrained moduli can be expressed as a Bosl and Nur (2002) short term poro-elastic relaxation in earthquake fracturing.

The undrained response (Δm = 0) implies a causal relationship between the pore pressure and the full hydrostatic stress on an element given by the Skempton coefficient B

$$\Delta P = -B\, \frac{\Delta\sigma_{kk}}{3} \qquad (A5)$$

Where

$$B = \frac{\frac{1}{K} - \frac{1}{K'_S}}{\frac{v_0}{K_f} + \frac{1}{K} - \frac{1}{K'_S} - \frac{v_0}{K''_S}} \qquad (A6)$$

The undrained Poisson ratio is obtained by substitution from (A6) for undrained state into (A1)

$$\nu_u = \frac{3\nu + B\,(1-2\nu)\left(1 - \frac{K}{K'_s}\right)}{3 - B(1-2\nu)\left(1 - \frac{K}{K'_s}\right)} \qquad \text{(A7)}$$

ν_u ranges between $[\nu, 1/2]$

Hence, the instantaneous elastic response can be expressed by:

$$2G\Delta\varepsilon_{ij} \equiv \Delta\sigma_{ij} - \frac{\nu_u}{1 + \nu_u}\, \Delta\sigma_{kk}\, \delta_{ij} \qquad (A8)$$

The porous medium constitutive equations can be expressed by a combination of drained and undrained poro-elastic response (Rice and Clearly., 1976):

$$\begin{cases} 2G\varepsilon_{ij} = \sigma_{ij} - \dfrac{\nu}{1+\nu}\,\sigma_{kk}\,\delta_{ij} + \dfrac{3(\nu_u - \nu)}{B\,(1+\nu)(1+\nu_u)}\,P\,\delta_{ij} \\ m - m_0 = \dfrac{3\,\rho_0(\nu_u - \nu)}{2GB\,(1+\nu)(1+\nu_u)}\,\left[\sigma_{kk} + \dfrac{3}{B}\,P\right] \end{cases} \qquad (A9)$$

Where summing for i = j the relation between the mean stress and the pore pressure relaxation is given by (Rice and Clearly, 1976):

$$\nabla^2\ \left[\sigma_{kk} + \frac{6(\nu_u - \nu)}{B\,(1-\nu)(1+\nu_u)}\,P\right] = 0 \qquad (A10)$$

As postulated by Nur and Booker (1972), the aftershocks production must consider the effect of pore pressure where the Coulomb stress change is defined as a time-dependent process and includes both pore pressure and stress state surrounding the fault zone. Piombo et al [2005] show that for a short time post-seismic response, the fluid effect is able to increase or decrease the Coulomb stress change. This observation correlates with the fact that the change to the shear stress caused by pore fluid diffusion is significant and may be strongly coupled to pore pressure. The pore pressure induced by the initial dislocation can be computed as $P = -B\sigma$ in undrained condition. Consequently, the stress change induced by pore fluid diffusion must satisfy the compatibility equation (A10).

In order to compute this effect just after an earthquake, Bosl and Nur (2002) imposed another boundary condition based on the fact that pore pressure equilibrium far from the source is a simple solution of the Rice and Cleary (1976) problem and it takes the following for:

$$[\,A\,P + \sigma] = 0 \qquad (A11)$$

$$A = \frac{2(\nu_u - \nu)}{B(1-\nu)(1+\nu_u)}$$

and σ is the change in stress field (due to the pore fluid diffusion) related to the initial stress induced by fault rupture (Bosl and Nur, 2002):

$$\frac{\sigma}{\sigma_{init}} = \frac{(\nu_u - \nu)}{(1-\nu)(1+\nu_u)} \qquad (A12)$$

This equation confirms that the postseismic mean stress change induced by pore pressure relaxation may increase or decrease in agreement with the initial mean stress caused by the fault rupture. Equation (A12) can be considered as an instantaneous response in the context of local equilibrium (Bosl and Nur, 2002).

According to Rice and Clearly (1976), the local pressure equilibrium over time is quite short by comparison to that needed for induced Darcy flows to achieve global pressure equilibrium over an entire deformed region. The mean stress due to the pore fluid diffusion in equation (A12) can be considered as an "instantaneous response" in the context of local equilibrium.

References

Biot, M. A., 1941. General theory of three-dimensional consolidation, *J. Appl. Phys.*, 12, 155-164.

Biot, M. A., 1955. Theory of elasticity and consolidation for a porous anisotropic solid, *J. Appl. Phys.*, 26, 182-185.

Bosl, W. J., & Nur, A., 2002. Aftershocks and pore fluid diffusion following the 1992 Landers earthquake, *J. Geophys. Res.*, 107, B12, 2366, doi:10.1029/2001JB000155.

Nur, A., & Booker, J.R., 1972. Aftershocks caused by pore fluid flow? *Science*, 25, 175 (4024), 885-7.

Rice, J.R., & Cleary M.P., 1976. Some basic stress diffusion solutions for fluid-saturated elastic porous media with compressible constituents, *Review of Geophysics and Space Physics*, 14, No. 2.

Appendix B: relationship between the poro-elastic model and the 2004 earthquake triggering

To perform our analysis and modelling on i) the poro-elastic effect in triggering seismic sequences, and ii) the influence of the mean stress induced by the isotropic (i.e., poro-elastic) model (rather than the normal stress attributed to the constant apparent friction model at the 2004 earthquake rupture), we compute the response of these two models subjected to a local maximum horizontal compressive stress (SH_{max}) acting in a local rupture zone and we study the influence of the poro-elastic effect on the Coulomb stress change.

In the tectonic model of Figure S4, we consider a scenario of tectonic loading in the epicentre area of the 2004 earthquake before the rupturing process, we assume that the strike slip faults are weaker than the surrounding reverse faults. For the Trans-Alboran Shear zone, Ibanez et al (2007) suggest that the SH_{max} deviation with respect to the regional stress field results from clockwise rotation with moderate to significant value (36°-78°). Consequently, the angle between SH_{max} and the 2004 right lateral strike slip faults is estimated to β = 70°. In our case, the SH_{max} represents the compressive stress applied to local fault sources of the Central Rif Block with respect to the Neogene and Quaternary clockwise rotation of the Oriental Rif Bloc (Tahayt et al., 2009; Ibanez et al., 2007). Combining the geodetic (GPS and InSAR) results and the tectonic model obtained by different authors (Akoglu et al., 2007; Tahayt et al., 2009), the stress distribution and block rotation seem to be controlled by a thick sedimentary accumulation (including tectonic nappes) where the active strike slip deformation accommodates earthquake ruptures (with right or left-lateral shearing) within the Trans-Alboran shear zone (Ibanez et al., 2007).

If we consider that the crust surrounding the 2004 earthquake rupture approaches the threshold for reverse faulting, the change in the Coulomb failure criterion per increment of tectonic loading $\Delta\sigma_1 = \Delta SH_{max}$ on the 2004 right-lateral strike-slip rupture plane according to the isotropic model can be expressed by the combination of shear, normal and pore pressure change contributions as given by Beeler et al (2000):

$$\frac{\Delta CFF}{\Delta\sigma_1} = \frac{(1-\upsilon)sin2\psi}{2} - \frac{\mu}{2}[1+\nu+(1-\nu)cos2\psi] + \frac{\mu B(1+\upsilon)}{3} \quad (B1)$$

Where the shear stress ($\Delta\tau$), the normal stress ($\Delta\sigma_n$) and the mean stress ($\Delta\sigma_m$) contributions are given by

$$\Delta\tau = \Delta\sigma_1\left(\frac{(1-\upsilon)sin2\psi}{2}\right); \quad \Delta\sigma_n = \Delta\sigma_1\left(\frac{1+\upsilon+(1-\upsilon)cos2\psi}{2}\right);$$

$$\Delta\sigma_m = \Delta\sigma_1\left(\frac{1+\upsilon}{3}\right)$$

The Coulomb Failure Function per increment of compressive stress load for a constant effective friction coefficient μ' becomes a contribution of shear and normal stresses (Beeler et al., 2000) as follows:

$$\frac{\Delta CFF}{\Delta\sigma_1} = \frac{(1-\upsilon)sin2\psi}{2} - \frac{\mu(1-B)}{2}[1+\nu+(1-\nu)\cos(2\psi)] \quad (B2)$$

where $\Delta\tau = \Delta\sigma_1\left(\frac{(1-\upsilon)sin2\psi}{2}\right)$; $\Delta\sigma_n = \Delta\sigma_1\left(\frac{1+\upsilon+(1-\upsilon)cos2\psi}{2}\right)$

Here, we consider that there is no stress perturbation due to the fault interaction (at pre-1994 field conditions), for a misdirected 2004 earthquake rupture geometry (ψ =20°; Figure S4). For a typical laboratory value (0.6, 0.8) of internal friction coefficient the normal stress change increases regardless of the Skempton pore pressure coefficient *B*. If the isotropic model is chosen as representative, our tectonic model stipulates that the increase of normal stress from μ = 0.6 to 0.8 implies a decrease in the Coulomb stress change which makes earthquake ruptures act in stable domain. Taking the case of ψ =20° (Figure S4) as a plausible local stress representation at a given depth for the 2004 rupture and for an isotropic (poro-elastic) model, a low friction coefficient is required for tectonic loading to move the fault toward a positive ΔCFF even if B = 1. For a constant friction model, μ can have any value if B = 1.

The isotropic model seems to be more representative of the failure process for strike slip faults in a transpressive regime and also able to reproduce the poro-elastic contribution due to an earthquake stress perturbation near a fault zone. The isotropic model is more sensitive to the mean stress change due to the short term poro-elastic effect and in fact more representative of the poro-elasticity than the constant apparent friction model. In order to give a more realistic representation of the short-term post-seismic stress change, the Coulomb stress change is computed by adding the contribution of the mean stress change (Figure 3b) as estimated by Bosl and Nur (2002).

References

Akoglu, A. M., Cakir, Z., Meghraoui, M., Belabbes, S., El Alami, S.O., Ergintav, S., & Akyüz, H.S., 2006. The 1994–2004 Al Hoceima (Morocco) earthquake sequence: Conjugate fault ruptures deduced from InSAR, *Earth Planet. Sci. Lett.*, 252, 467–480

Beeler, N.M., Simpson, R.W., Hickman, S.H. & Lockner, D.A., 2000. Pore fluid pressure, apparent friction and Coulomb failure, *J. Geophys. Res.*, 105, B11, 25,533-25,542.

Bosl W.J., & Nur A., 2002. Aftershocks and pore fluid diffusion following the 1992 Landers earthquake, *J. Geophys. Res.*, 107, B12, 2366, doi:10.1029/2001JB000155.

Ibanez, F., Soto, J.I., Zoback M.D., & Morales, J., 2007. Present-day stress field in the Gibraltar Arc (western Mediterranean), *J. Geophys. Res.*, 112, doi:10.1029/2006JB004683.

Piombo, A., Martinelli, G. & Dragoni, M., 2005. Post-seismic fluid flow and Coulomb stress changes in a poro-elastic medium, *Geophys. J. Int.*, 162, 507–515, doi: 10.1111/j.1365-246X.2005.02673.x.

Rice J.R., 1992. Fault stress states, pore pressure distributions, and the weakness of the San Andreas fault, B., in Evans, B., and Wong, T. F., eds., Fault mechanics and transport properties of rocks: New York, Academic Press, 475-504

Tahayt, A., Feigl, K.L., Mourabit, T., Rigo, A., Reilinger, R., McClusky, S., Fadil, A., Berthier, E., Dorbath, L., Serroukh, M., Gomez, F., & Ben Sari, D., 2009, The Al Hoceima (Morocco) earthquake of 24 February (2004) analysis and interpretation of data from ENVISAT ASAR and SPOT5 validated by ground-based observations, Remote Sens. Environ, 113, 306–316.